Master's thesis

A Novel Route to
Colloidal InSb Quantum Dots

Mariska de Ruiter

Supervisors:
Serena Busatto M.Sc.
Dr. Celso de Mello-Donegá

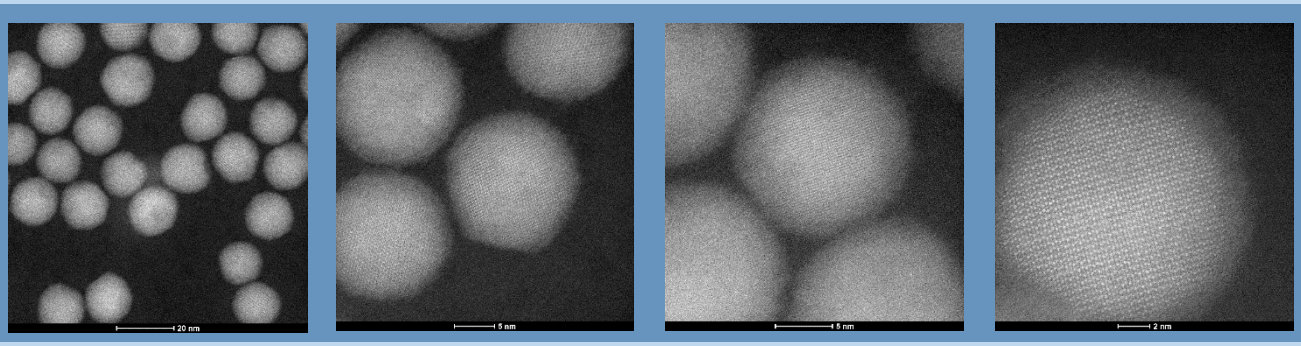

Condensed Matter and Interfaces
Debye Institute for Nanomaterials Science

Utrecht University

February 28th, 2019

The images on the front page are high resolution transmission electron microscopy images of 15 nm-sized colloidal InSb quantum dots that were synthesized according to the method that is presented in this thesis. Image courtesy of W. Albrecht and S. Bals (EMAT Antwerp).

Abstract

The III-V semiconductor material InSb has an unusually large exciton Bohr radius (viz., 60 nm). Therefore, InSb quantum dots can be strongly quantum confined at larger sizes than most semiconductors. This allows their band gap to be tuned across a broad range of energies spanning from the mid- to the near-infrared. Consequently, InSb quantum dots are a promising material for application in devices such as infrared detectors and quantum dot solar cells. However, despite their great potential, the colloidal synthesis of InSb quantum dots is still severely underdeveloped. Existing preparation routes rely on the synthesis of the precursor compounds through elaborate methods. In this thesis, a novel synthesis route to colloidal InSb quantum dots is presented in which exclusively commercially available precursors are used. By *in situ* formation of a single-source precursor we were able to synthesize highly crystalline and stoichiometric colloidal InSb quantum dots. We determined the size-dependence of the InSb quantum dot band gap using steady-state near-infrared absorption spectroscopy. Transient absorption and photoluminescence spectroscopic measurements indicated that charge carriers in InSb quantum dots are quickly localized at trap states.

Contents

Chapter 1: Introduction

In the '80s, Louis Brus discovered that the behaviour of semiconductor crystals is significantly altered when their dimensions are reduced to the nanoscale.[1] At this length scale, important characteristics such as the band gap, melting temperature and magnetism of the material become size-dependent due to quantum confinement effects.[2] This means that the properties of the material can be tuned to the desired values by simply adjusting the size of the nanocrystals while keeping their composition constant. This ground-breaking discovery led to extensive research on these so-called quantum dots. Over the past decades, scientists learned to synthesize quantum dots in liquid dispersions (i.e. using bottom-up colloidal methods). This colloidal preparation method offers great control over the quantum dots' size and shape. Moreover, the solution processing techniques used to synthesize colloidal quantum dots are inexpensive, facile and scalable.[2] The field has developed at such an astonishing rate that at present, only 35 years after Brus' discovery, the first consumer devices containing colloidal quantum dot technology have entered the market. Since 2015, Samsung sells television screens in which quantum dots prepared through colloidal routes improve display brightness and colour gamut.[3] In the near future, colloidal quantum dots may also be incorporated in devices such as LEDs, solar cells or luminescent solar concentrators. Additionally, colloidal quantum dots are promising for application in the fields of *in vivo* imaging and photothermal therapy.

To date, research has primarily focused on II-VI and IV-VI semiconductor quantum dots such as CdSe and PbSe. The group of III-V semiconductor quantum dots is still scarcely studied and a thorough understanding of their chemistry and physics is lacking. This is mainly due to the largely covalent nature of III-V semiconductors, which renders III-V quantum dots extremely challenging to synthesize.

The most fascinating among the III-V semiconductors is commonly regarded to be indium antimonide (InSb) since it possesses a number of extreme properties. Bulk InSb has the smallest band gap of all binary semiconductors (0.17 eV).[4] Additionally, its electron mobility is extremely high (78000 $cm^2/V{\cdot}s$[4]) and its thermal conductivity and exciton binding energy are very low (16 $W/m{\cdot}K$[5] and 0.5 meV[4], respectively). Furthermore, the exciton Bohr radius of InSb is as large as ~60 nm.[4] This means that InSb quantum dots can experience very strong quantum confinement already at relatively large sizes. This allows the InSb quantum dot band gap to be tuned across a wide range of energies from the mid- to near-infrared spectral region.

A number of applications can be envisioned for InSb quantum dots. Their narrow band gap, high electron mobility and low thermal conductivity make them suitable for application in infrared detectors, high-frequency electronics and thermoelectric power conversion devices. Furthermore, small InSb quantum dots may offer a low-toxic alternative to PbSe quantum dots in solution-processable quantum dot solar cells.

Despite their great potential, the colloidal synthesis of InSb quantum dots is still severely underdeveloped. In the past decade, a total of four papers was published on this subject.[4][6-8] Only the articles by Liu *et al.*[4] and Yarema *et al.*[6] present viable synthesis routes to high quality InSb quantum dots. However, both methods rely on the preparation of silylamide precursors, which requires lengthy reaction times and multiple purification steps. In this thesis, a new procedure will be set forth in which highly crystalline and stoichiometric quantum dots are prepared using only commercially available precursor compounds.

The thesis is structured as follows. Chapter 2 discusses the theoretical background that is required to understand the contents of this thesis. The experimental procedures related to the synthesis, post-synthetic treatment and characterization of InSb quantum dots are described in Chapter 3. In Chapter 4, the outcome of these experiments is discussed in detail. In section 4.1, we take a closer look at the precursor solution. In section 4.2, the reaction products are presented and a mechanism for the nucleation and growth of the colloidal InSb quantum dots is proposed. Section 4.3 elaborates on the post-synthetic treatment procedure. The optical features of the InSb quantum dots are discussed in section 4.4. Finally, Chapter 5 presents a conclusion and outlook in which we set forth our future plans regarding this study.

Chapter 2: Theoretical background

2.1 What are nanomaterials?

Nanomaterials are materials that have a length scale within the nanoregime (≤ 100 nm) in one or more dimensions.[9] The exciting feature of such materials is that their intrinsic properties may be very different from those of the bulk material and highly dependent on the size of the nanoparticle. This can be attributed to two important nanoscale effects, namely (1) scaling effects and (2) spatial confinement effects.

When the size of a particle is decreased, the number of atoms that constitutes the particle becomes smaller and smaller.[9] At the same time, the fraction of the atoms that is located at the particle surface steadily increases. In other words, the surface/volume ratio increases as the particle size decreases. Consequently, the surface energy, which is due to the unsatisfied chemical bonds of the surface atoms, has an increasing influence on the total free energy. This leads to a rise in reactivity, the ability to form colloidal dispersions and possibly the formation of crystal structures that are only metastable for the bulk material.

Spatial confinement effects start to influence the nanoparticle properties when the size of the nanoparticle becomes comparable to or lower than a characteristic length scale of a physical entity or phenomenon.[9] For the plasmon resonance in metal nanoparticles, for example, this characteristic length scale is the electron mean free path. In semiconductor nanoparticles, quantum confinement renders the material's properties size-dependent when their radius becomes smaller than the exciton Bohr radius (a_0). Section 2.2 presents a more in-depth discussion of quantum confinement in semiconductor nanoparticles.

2.2 Quantum confinement effects in semiconductor nanoparticles

The exciton Bohr radius (a_0) describes the spatial extension of an exciton that is generated through absorption of light by semiconductor materials.[9] Its value is highly dependent on the material under consideration. An example of a semiconductor with a small exciton Bohr radius is ZnS (a_0 = 1.5 nm[10]). The exciton Bohr radius of InSb, on the other hand, is considered to be very large (a_0 = ~60 nm[4]). When the nanocrystal radius becomes equal to or smaller than a_0, the nanoparticle becomes spatially confined. As a result, the kinetic energy of the nanocrystal increases. This phenomenon is called quantum confinement. Spherical nanocrystals experience quantum confinement in all directions and are therefore considered to be zero-dimensional. For that reason, such spherical nanocrystals are also called quantum dots.

The electronic structure of a bulk semiconductor material consists of two bands of very closely spaced energy levels that are separated from each other by a band gap. The lower band is called the valence band and the upper band is called the conduction band. The valence band is filled with electrons while the conduction band is empty. Figure 2.1 illustrates the effects of quantum confinement on the electronic structure of the semiconductor nanocrystal. The electrons inside the nanocrystal are described according to the particle-in-a-box model. In this model, the potential energy inside the particle is taken to be zero, and the potential energy outside the particle is taken to be infinitely large. When the nanocrystal size is reduced to a value below $2a_0$, the quantum confinement potential of the particle-in-a-box causes the closely spaced states to rise in energy as depicted in Figure 2.1 (a). Figure 2.1 (b) shows how this effect influences the electronic structure of the nanocrystal. The band gap energy increases and discrete energy levels appear near the band

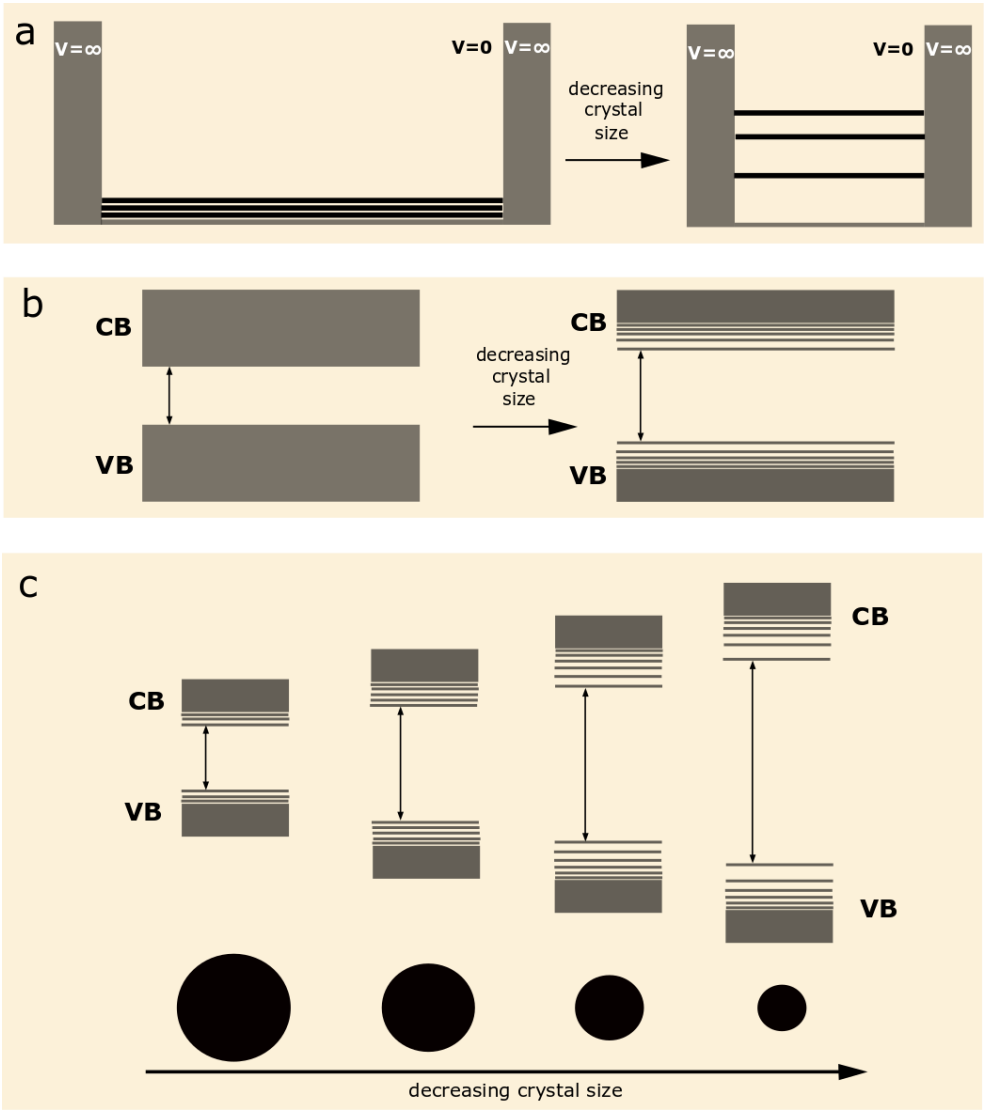

Figure 2.1 The electronic effects of quantum confinement in semiconductor nanocrystals. (a) The quantum confinement potential causes the energy levels of the band gap to shift. (b) The effects of quantum confinement on the semiconductor electronic structure. (c) The resulting size-dependence of the quantum dot bandgap.

gap. As depicted in Figure 2.1 (c), when the size of the quantum dot is further decreased, this effect becomes more pronounced and the band gap energy increases even more. In this way, the quantum dot band gap can be tuned by adjusting the size of the nanocrystals.

A more quantitative insight into the size-dependence of the quantum dot band gap can be obtained by solving the Schrödinger equation for the particle-in-a-box model. From the forthcoming expression for the energy levels of the system it can be deduced that the band gap of a quantum dot with diameter d can be approximated with the following formula:

$$E_g(d) = E_g(\infty) + \frac{\hbar^2 \pi^2}{2d^2}\left[\frac{1}{m_e^*} + \frac{1}{m_h^*}\right] - \frac{1.786e^2}{\varepsilon d}$$

where E_g is the band gap energy, $\hbar$ is the Planck constant, m_e^* is the effective electron mass, m_h^* is the effective hole mass, e is the elementary charge and ε is the effective dielectric constant.[11] The

first term equals the band gap energy of the bulk material. The second term is the confinement potential that is added to the bulk band gap energy when the nanocrystal is quantum confined. The third term represents the Coulomb interaction between the electron and the hole that are forced to be nearer to each other upon decreasing the size of the nanocrystal. However, due to the large dielectric constant ε of semiconductor materials, the charges of the electron and the hole are shielded to such an extent that this interaction is very weak.

2.3 Optical properties of quantum dots

The effect of quantum confinement is clearly demonstrated in the optical properties of the quantum dots. When a quantum dot is illuminated by photons with an energy that is equal to or higher than the band gap energy, the quantum dot can absorb a photon to promote an electron from the valence band to the conduction band. The positive charge that is then generated in the valence band is referred to as a hole, and the electron-hole pair is called an exciton. The energies of the photons absorbed by the quantum dots are highly dependent on the band gap energy. These energies will blueshift upon decreasing the size of the quantum dots. Figure 2.2 (a) illustrates this concept for CdTe quantum dots. Remarkably, the absorption spectra presented in Figure 2.2 (a) show multiple distinct peaks. These peaks are a consequence of the discrete energy levels at the top of the valence band and the bottom of the conduction band. The lowest energy peak corresponds to the $1S_h$-$1S_e$ transition, the higher energy peaks to the $1P_h$-$1P_e$ and $1D_h$-$1D_e$ transitions, respectively (Figure 2.2 (b)).[9]

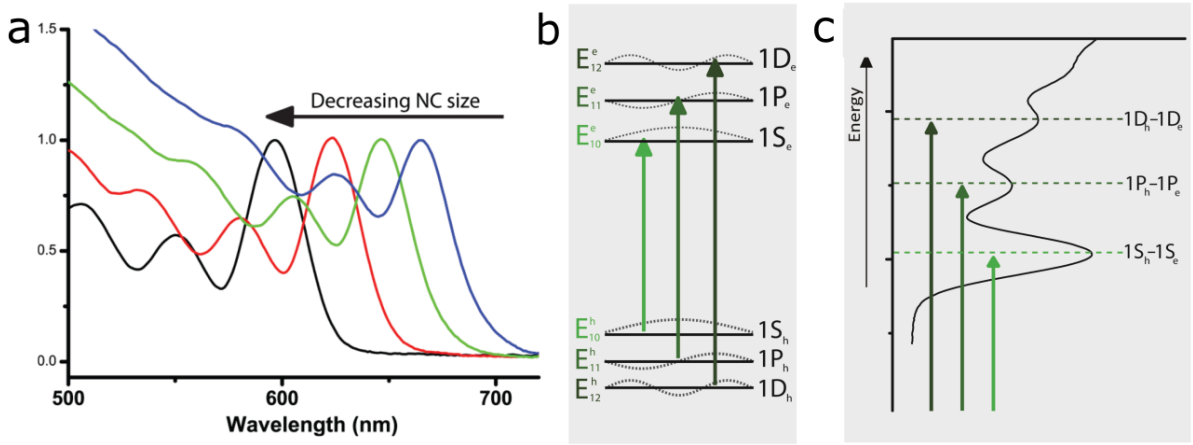

Figure 2.2 (a) CdTe quantum dots with decreasing size show a blueshift in their absorption spectrum. (b), (c) The peaks in the absorption spectra are a consequence of the discrete energy levels at the band edges. Adapted from Ref. [9]

In order to observe discrete peaks in the absorption spectrum, the sample must consist of an ensemble of quantum dots with a sufficiently narrow size polydispersity. Any degree of polydispersity will cause the absorption peaks to broaden, ultimately making them indistinguishable from each other. This effect is most pronounced for strongly confined quantum dots since their absorption wavelength is extremely sensitive to small deviations in quantum dot size.

The electron-hole pair that is generated upon absorption of a photon can recombine in a radiative or a non-radiative way (Figure 2.3).[9] In the radiative recombination pathway, the quantum dot relaxes back to its ground state by emission of a photon. This radiation is called photoluminescence and may be useful for many applications. Alternatively, the quantum dot can relax back to its ground state non-radiatively by the promotion of vibrations. Non-radiative combination is often mediated by

inter-band gap energy states caused by impurities and defects in the quantum dot crystal. An important source of defects is the quantum dot surface. Since the atoms at the quantum dot surface are not completely surrounded by neighbouring atoms like the atoms at the core of the quantum dot, they have unsatisfied chemical bonds. In case these so-called dangling bonds are not passivated by ligand molecules, they lead to inter-band gap energy states. Surface passivation by ligand molecules is discussed in more depth in section 2.5.

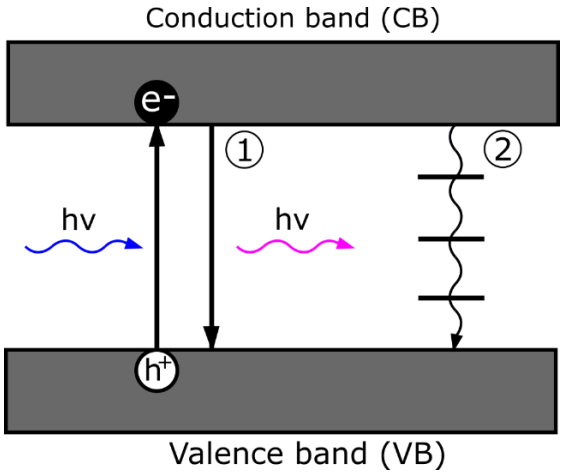

Figure 2.3 After an electron is promoted to the valence band under absorption of a photon, it can relax back to the ground state via radiative (1) or non-radiative (2) decay. Adapted from Ref. [9].

One strategy to eliminate dangling bonds at the quantum dot surface is the overgrowth of the surface with a heteroepitaxial shell of a suitable material. A suitable shell material should meet two demands. First of all, in order to prevent leakage of the charge carriers into the shell material, the band gap of the core semiconductor should lie entirely within the band gap of the shell material as depicted in Figure 2.4 (a).[12] In the resulting core-shell quantum dot, the electron and hole wave functions are confined in the core quantum dot (Figure 2.4 (b)) so that the optical properties of the quantum dots remain virtually unaltered. The second demand is that the lattice mismatch between the shell and the core materials is small so that the interfacial strain between the two materials is limited. The passivation of the surface states reduces the non-radiative recombination pathways of the exciton and thereby increases the quantum dots' photoluminescence yield.

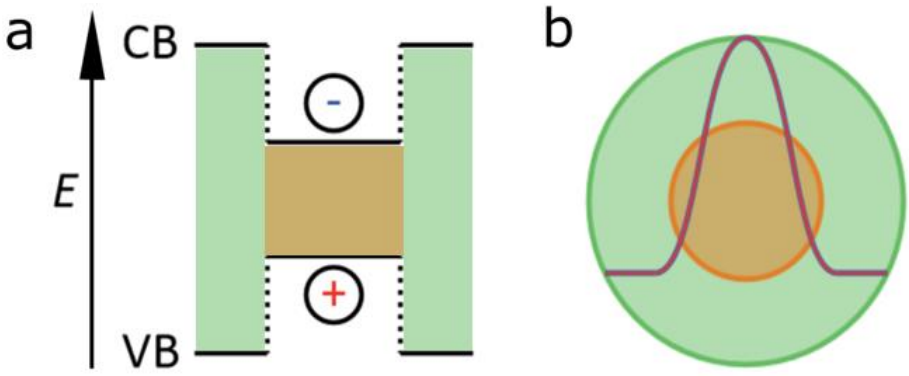

Figure 2.4 Charge carrier localization in a core-shell quantum dot. (a) When the band gap of the core semiconductor lies entirely within the band gap of the shell material, the photogenerated charge carriers remain localized in the core semiconductor. (b) The exciton wave function is confined in the core of the core-shell quantum dot. Adapted from Ref [12]

2.4 Formation of colloidal quantum dots

Since their discovery, many efforts have been made to develop colloidal synthesis methods for highly crystalline quantum dots with small size and shape dispersions. Most of these synthesis methods involve the injection of a cold mixture of precursor molecules into a hot coordinating solvent. This method is commonly referred to as the hot injection method.[9] According to the classical nucleation and growth theory as formulated by LaMer[13], the formation of quantum dots contains three stages: (I) the induction period, (II) the nucleation period and (III) the growth period. These stages are illustrated in Figure 2.4.

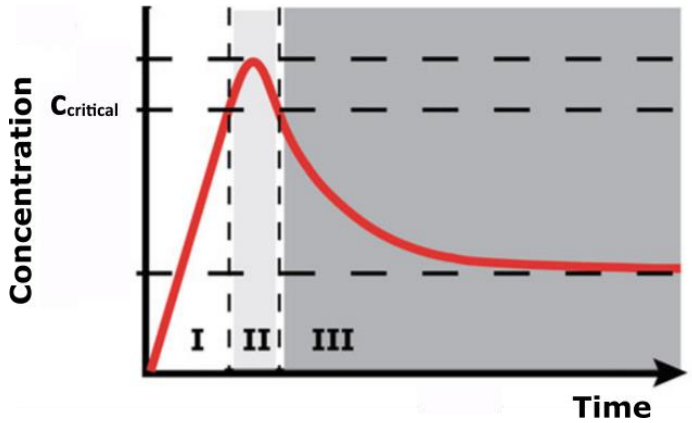

Figure 2.4 The three widely recognized stages in quantum dot synthesis using the hot injection method (I - induction period, II - nucleation period and III - growth period). Adapted from Ref. [9].

The start of the induction period is marked by the injection of the precursor compounds into the hot reaction solvent. If the temperature is sufficiently high, the precursors will react to form monomers, which are the basic building units of the crystal. For semiconductor quantum dots, this monomer is a cation-anion pair – for CdSe quantum dots, for example, this will be one [CdSe] unit. At this stage, the monomers may form unstable clusters that are too small to be capable of growing and will therefore redissolve.[9]

When the concentration of monomers is sufficiently high, the monomers form clusters that are large enough to be capable of growing into mature nanocrystals. These clusters are called nuclei. Once the nuclei are formed, they immediately enter the growth stage, in which they grow through monomer addition. The size of the nanocrystal will continue to increase until most of the monomers are used up or until the solution is cooled to such an extent that no more monomer addition can take place.[9]

The greatest challenge in quantum dot synthesis is the control over the mean size and size distribution of the product nanocrystals. The mean size of the quantum dots is controlled by the number of nuclei that form in stage II, the amount of remaining monomers after stage II and the diffusion coefficient of the monomers. The width of the particle-size distribution is thought to be dependent on the time window to which the nucleation is confined.[14] In order to obtain the narrowest size distribution, the nucleation stage should be as short as possible. In that way, all nuclei start growing at the same time and will therefore end up having the same size.[15] The end of the nucleation stage is achieved when the concentration of free monomers drops below the critical value.[9] Therefore, in order to make the time window of the nucleation stage as narrow as possible, the monomers must be consumed as fast as possible by the nucleation and growth processes.

A non-classical growth process is growth through the coalescence of nanocrystals. Growth through coalescence may take place simultaneously with classical growth processes or occur independently of classical growth. This growth mechanism is claimed to be dominant in cases where the monomer formation is much faster than the classical growth process.[16] The coalesced particles may initially be polycrystalline but will usually recrystallize to single crystals. Smaller particles are more likely to grow through coalescence than larger particles since they have larger volume-to-surface ratios and increased mobility.[15]

Growth through coalescence is fundamentally different from growth through monomer addition. For growth through monomer addition, the rate-limiting step is either the addition of the monomer to the quantum dot or the diffusion of the monomers onto the quantum dot surface.[9] Growth through coalescence, on the other hand, is completely governed by the frequency with which the quantum dots collide. Whereas growth through monomer addition leads to a smooth and continuous quantum dot size increase, the size increase of quantum dots that grow through coalescence occurs in a stepwise manner.[15]

2.5 The role of the capping ligands

Colloidal quantum dots are usually coated with a layer of ligand molecules that allows them to form stable colloidal dispersions. These ligands are often amphiphilic organic molecules consisting of a polar head group (for example acid, thiol or amine groups) and a long apolar hydrocarbon chain.[9] The polar head group binds to the quantum dot surface and the apolar chain points outwards into the dispersing medium. These long chains prevent the quantum dots from coming sufficiently close to each other for the van der Waals forces to take over and cause irreversible aggregation. The bond between the quantum dot and the ligand often has a dynamic nature: in equilibrium conditions, the ligands alternate between their bound states and moving freely in solution.[17]

During the synthesis, the presence of ligands is necessary to help the monomers and nuclei stay in solution. However, the nature and concentration of ligands affect the quantum dot nucleation and growth to an extent much larger than one might expect. The ligands may enhance the decomposition rate of the precursor or increase the stability of the monomer units.[9] Moreover, the ligands compete with the monomers for adsorption onto the surface sites. When the bond between the ligand and the quantum dot surface is too strong, it may block the surface of the quantum dot and in that way inhibit the crystal growth. Therefore, weakly bound ligands are most commonly used during the synthesis.

After the synthesis, there is no more demand for available surface sites. In order to increase the stability of the quantum dots, the weakly bound ligands can be exchanged for stronger ligands. Strongly bound ligands are essential to keep the quantum dots stable through the subsequent post-synthetic treatments such as purification, shell growth or cation exchange.

Chapter 3: Experimental

3.1 Chemicals

Oleylamine (OLAM, 70%), octadecylamine (ODA, ≥99.0%), hexadecylamine (HDA, 98%), dodecylamine (DDA, ≥99.0%), octylamine (97%), toluene (anhydrous, 99.8%), tris(dimethylamido)antimony(III) ($Sb[NMe_2]_3$, 99.99%), indium(III)chloride ($InCl_3$, 98%), lithium triethylborohydride (Super-Hydride®, 1 M in THF), 1-butanol (anhydrous, 99.8%), methanol (anhydrous, 99.8%), acetonitrile (ACN, anhydrous, 99.8%), methyl acetate (MeOAc, anhydrous, 99.5%), oleic acid (90%), 1-dodecanethiol (DDT, ≥98%) and tetrachloroethylene (TCE, anhydrous, ≥99%) were purchased from Sigma Aldrich. Dioctylether (DOE, 99%) and ethanol (anhydrous, 96%) were purchased from Alfa Aesar. All chemicals were used as received except for oleylamine, oleic acid and triethylborohydride.

Oleylamine and oleic acid were degassed before use. The degassing was performed at 100 °C under reduced pressure for a duration of over 4 hours. Due to varying vacuum pump strength, the pressure that was achieved varied between $1 \cdot 10^{-3}$ and $1 \cdot 10^{-2}$ bar.

The solvent of triethylborohydride was exchanged for DOE by mixing equal volumes of DOE and triethylborohydride in THF and degassing the mixture at room temperature using standard Schlenkline techniques until the volume of the mixture was reduced by half.

3.2 Synthesis methods

All experiments were carried out in a glovebox under nitrogen (H_2O and O_2 < 2 ppm).

The precursor solution

2 ml toluene, 0.497 g OLAM (1.86 mmol) and 0.200 g $Sb[NMe_2]_3$ (0.78 mmol) were mixed together yielding a bright yellow solution. 0.173 g $InCl_3$ (0.78 mmol) was added and dissolved under stirring and heating the mixture to 50 °C for a duration of one minute. The resulting solution is clear and bright yellow.

Synthesis of colloidal InSb quantum dots

In a typical synthesis, 7 ml OLAM was heated to 240 °C in a round-bottom flask under constant stirring. At this temperature, 0.98 ml Super-Hydride® in DOE (1.0 M, 0.84 mmol) was injected in a dropwise manner. During the injection, OLAM acquired an orange colour. After the injection, the temperature was kept steady at 240 °C for a duration of Δt_{wait} = 10 minutes. Subsequently, 0.18 ml of the precursor solution was injected using a Finn pipette. After keeping the temperature at 240 °C for 4 minutes, the reaction solution was transferred to four cold vials each containing 1 ml toluene using a Pasteur pipette.

The reaction container, reaction time and temperature, solvent, amount of Super-Hydride®, Δt_{wait} and precursor ratio were varied in order to study their influence on the reaction products.

Post-synthetic treatment

A typical treatment consisted of three stages: the colloidal stabilization stage, purification stage and size-selective precipitation stage.

The colloidal stabilization

- Method A: For each vial, 0.25 ml DDT and 0.25 ml oleic acid were added to the reaction solution 1 and 3 minutes after the quenching of the reaction into toluene, respectively. The solution was kept at room temperature for 30 minutes.
- Method B: For each vial, 0.25 ml oleic acid was added to the reaction solution 2 minutes after the quenching of the reaction into toluene. The solution was kept at room temperature for 30 minutes.

The purification

3 ml BuOH and 3 ml MeOH were added to the reaction solution, causing the solution to become turbid. Centrifugation for 10 minutes at 2800 rpm yielded a black precipitate and colourless supernatant. The colourless supernatant was discarded and the black precipitate was redispersed in toluene yielding a stable suspension.

The size-selective precipitation

The purified sample was centrifuged for 10 minutes at 2800 rpm and any precipitate was separated from the supernatant and redispersed in toluene. To the supernatant, a small amount of MeOAc was added, after which the sample was centrifuged for 10 minutes at 2800 rpm and the precipitate was separated from the supernatant and redispersed in toluene. This cycle of (1) addition of small amounts of MeOAc to the supernatant, (2) centrifugation and (3) separation of the precipitate was repeated until the supernatant had become colourless. Typically, in order to obtain a precipitate from 1 ml of purified quantum dot dispersion, ~0.4 ml MeOAc was needed in the first cycles and ~1.0-5.0 ml MeOAc was needed in the later cycles.

3.3 Characterization

^{1}H and ^{13}C nuclear magnetic resonance (NMR) spectroscopy

A small amount of the compound under study was dissolved in 0.5 ml deuterated toluene so that the resulting solution had a concentration of around 30 mg/L. This solution was transferred to an air-sealed NMR sample tube. The ^{1}H and ^{13}C NMR measurements were performed using an Agilent MRF400 equipped with a OneNMR probe and Optima Tune system. The spectra were recorded using the following parameters: 400 MHz, 25 °C and a pulse repetition time of 25 seconds.

Fourier transform infrared (FTIR) spectroscopy

The compounds under study were dissolved in TCE and transferred to a quartz cuvette. Measurements were conductor on a BRUKER Vertex 70 apparatus equipped with a KBr/DLaTHS D301 detector.

Transmission electron microcopy, energy dispersive x-ray (EDX) spectroscopy and electron diffraction (ED)

The quantum dot dispersion was diluted with toluene until its colour was dark brown. This solution was dropcasted onto polymer-coated copper TEM grids under ambient conditions and analysed using several different microscopes. Images were acquired using a FEI Tecnai20 microscope operated at 200 keV, a FEI Tecnai20FEG microscope operated at 200 keV and a FEI TALOSF200X operated at 200 keV. Quantum dot sizes were deduced from the TEM images by measuring around 80 particles by hand using ImageJ software. High resolution TEM (HRTEM) was performed on an aberration corrected 'cubed' FEI Titan 60-300 microscope operated at 300 keV. The lattice spacings of the quantum dots were obtained from the HR-TEM images by taking the Fourier transform (FT) of the area of interest. EDX measurements were performed on a FEI Tecnai20FEG microscope operated

at 200 keV, a TALOSF200X microscope operated at 200 keV and an aberration corrected 'cubed' FEI Titan 60-300 microscope operated at 300 keV. Electron diffraction was performed on a FEI Tecnai20 microscope operated at 200 keV.

Near infrared (NIR) absorption spectroscopy

The quantum dot dispersion was transferred to a quartz cuvette and diluted with toluene until its colour was dark brown. Another quartz cuvette was filled with toluene from the same source and used as a reference. Absorption measurements were conducted on a Perkin Elmer Lambda 950 UV/Vis spectrometer in the wavelength range from 700 to 2000 nm. The positions of the peaks in the absorption spectra were determined as the wavelength for which the second derivative of the absorption curves have the minimum value.

Transient absorption (TA) spectroscopy

The quantum dot dispersion was transferred to a quartz cuvette and diluted with toluene until its colour was dark brown. An Yb:KGW oscillator (Light Conversion, Pharos SP) was used to generate 180 fs laser pulses with a 1028 nm wavelength and a frequency of 5 kHz. In order to obtain the pump probe pulses of 650 nm, the majority of the fundamental 1028 nm beam underwent non-linear frequency mixing in an Optical Parametric Amplifier (OPA) equipped with a second harmonic module (Light Conversion, Opheus). The remaining fraction of the fundamental 1028 nm beam was used to generate a broadband probe spectrum by supercontinuum generation in a sapphire crystal. The delay time of the probe beam was controlled by an automated delay-stage. The quantum dot solution was hit by the pump and probe pulses under a small relative angle (~8°). After transmission through the sample, the probe beam was collected at a detector (Ultrafast Systems, Helios).

Photoluminescence (PL) spectroscopy

Photoluminescence spectra were recorded on an Edinburgh Instruments FLS920 spectrofluorometer equipped with a 450 W Xe lamp as excitation source and double grating monochromators for both the excitation and the emission. The excitation wavelength was 600 nm. The spectrum was recorded over an emission range of 900-1750 nm with a step size of 2 nm and a dwell time of 1 second. A 830 nm long pass filter was fixed before the detector, which was a liquid N_2-cooled Hamamatsu R5509-72 photomultiplier tube. The spectra were corrected for the instrumental response. Measurements were carried out at temperatures of 298 K and 4 K. In order to carry out measurements at 4 K, the quantum dot solutions were transferred to a liquid cell. The liquid cell was mounted in a continuous He-flow cryostat and cooled to 4.1 K.

Chapter 4: Results and discussion

4.1 The precursor solution

This thesis describes the synthesis of high quality colloidal InSb quantum dots using the commercially available precursor compounds $InCl_3$ and $Sb[NMe_2]_3$. In order to fully appreciate this remarkable success, it is useful to get acquainted with the state-of-the-art of this field. Therefore, the next paragraphs discusses the four articles that have been published on the synthesis of colloidal InSb quantum dots.

The first article presenting the colloidal synthesis of InSb quantum dots was published by Liu *et al.* in 2012.[4] They proposed that the formation of InSb quantum dots takes place through In^0 and Sb^0 intermediates. Therefore, the preparation method needs to include a reduction step in which a strong reducing agent is added to the reaction solution. As a precursor for antimony, Liu *et al.* synthesized the silylamide compound $Sb[N(Si(Me)_3)_2]_3$. This compound was dissolved together with $InCl_3$ in trioctylphosphine. At room temperature, the resulting mixture was injected into a solution of the strong reducing agent $LiEt_3BH$ in oleylamine. This temperature was increased to 260 °C at a rate of 3 °C per minute after which the solution was annealed for 20 minutes. Using this method, Liu *et al.* produced high quality zinc blende InSb nanocrystals with sizes varying from 3.4 to 7.0 nm (Figure 4.1 (a)). They were able to tune the quantum dot band gap from 1.03 to 0.71 eV (Figure 4.1 (b)) and observed photoluminescence with a quantum yield of <1% at room temperature.

In 2013, Yarema *et al.* prepared colloidal InSb quantum dots in a likewise manner.[6] Their initial experiments showed that indium carboxylates are unsuitable precursors for In since they lack reactivity. $InMe_3$, on the other hand, reacted uncontrollably fast at temperatures exceeding 200 °C. Therefore, Yarema *et al.* synthesized the silylamide compound $In[N(Si(Me)_3)_2]_2$, which had a reactivity in between that of the indium carboxylates and $InMe_3$. In order to synthesize InSb quantum dots, they combined $In[N(Si(Me)_3)_2]_2$ with $Sb[NMe_2]_3$ in different reductive solvents. They developed a synthesis in trioctylphosphine in which the reaction mixture was heated from room temperature to 200 °C at a rate of about 15 °C per minute and subsequently annealed for 5 minutes. Additionally, they developed a synthesis in trioctylamine involving of the hot injection of the precursor compounds at 250 °C and annealing for 5 to 15 minutes at 200 °C. Using these methods, Yarema *et al.* obtained both wurtzite and zinc blende InSb quantum dots. The InSb quantum dot sizes ranged from 3.2 to 10 nm and the band gap was tuned from 1.0 to 0.7 eV (Figure 4.1 (c), (d)). They observed photoluminescence with a weak intensity.

In 2018, Crisp *et al.* attempted to synthesize InSb quantum dots by reacting In and Sb atoms in the +3 and -3 oxidation states, respectively.[8] In their standard preparation method, they injected $Sb[NMe_2]_3$ and a strong reducing agent into a solution of indium oleate in ODE at 165 °C and annealed at 185 °C for 3 minutes. They propose that Sb^{3+} is selectively reduced to Sb^{3-} *in situ*, after which it readily reacts with In^{3+}. This preparation method yielded InSb clusters with a diameter of 1 nm and distinct absorption peaks at 510 and 650 nm (Figure 4.1 (e), (f)). Their attempts to synthesize bigger nanocrystals had very limited success.

Although Liu *et al.* and Yarema *et al.* both present viable routes to colloidal InSb quantum dots, both of these methods rely on the synthesis of silylamide precursors. These syntheses are extremely time-consuming since they require lengthy reaction times and multiple purification steps. Therefore, a novel route towards colloidal InSb quantum dots using only commercially available precursors is highly desirable. The final article that is discussed in this section was published by Tamang *et al.* in 2015.[7] They attempted to synthesize InSb quantum dots using the commercially available

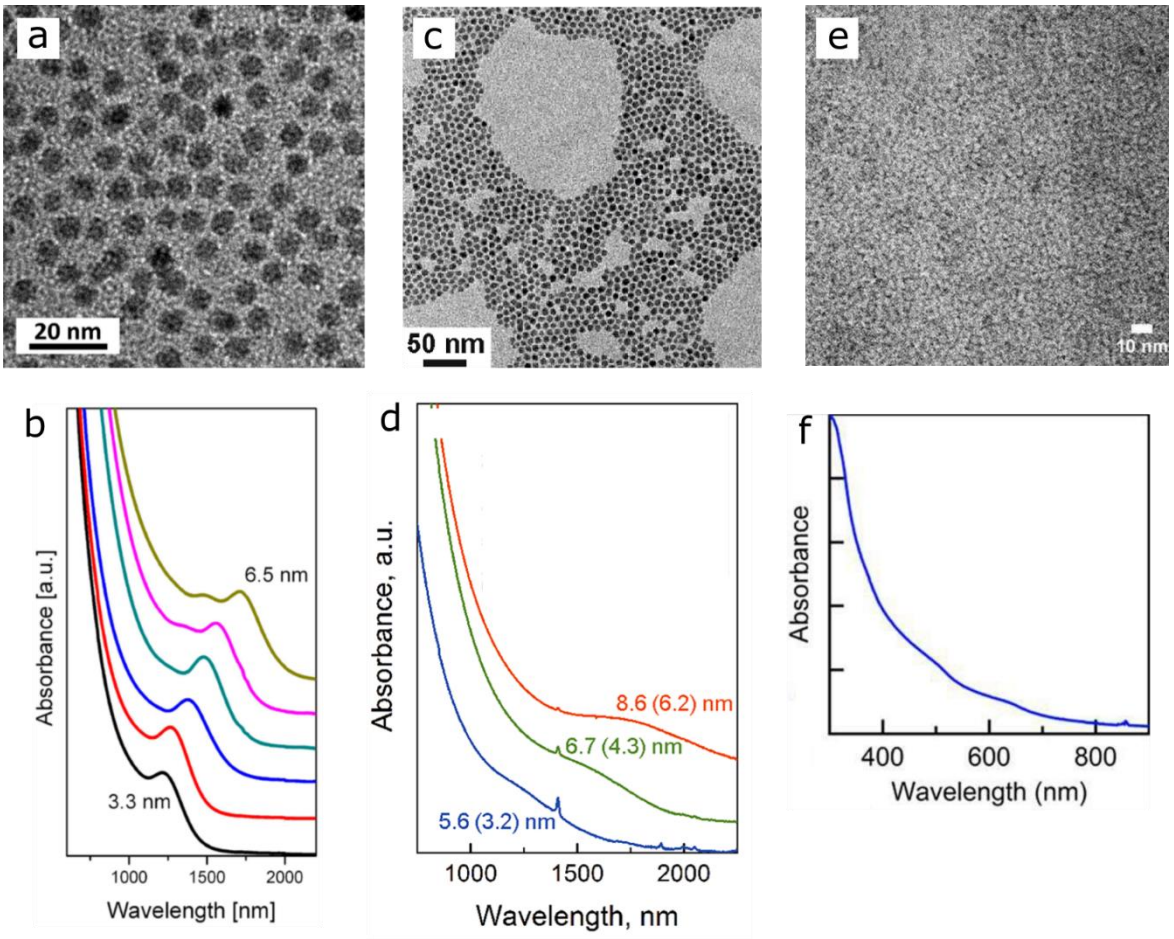

Figure 4.1: Results obtained on the syntheses of colloidal InSb quantum dots performed by Liu *et al.*[4], Yarema *et al.*[6] and Crisp *et al.*[8] (a), (b) TEM image and absorption spectra of the InSb quantum dots obtained by Liu *et al.* (c), (d) TEM image and absorption spectra of the InSb quantum dots obtained by Yarema *et al.* (e), (f) TEM image and absorption spectrum of the InSb clusters obtained by Crisp *et al.* Reproduced from Ref. [4], [6] and [8].

precursor compounds $InCl_3$ and $Sb[NMe_2]_3$ – the same precursor compounds as are used in the new preparation method presented in this thesis. They found that by injecting a reducing agent and the antimony precursor in trioctylamine containing the indium precursor at 250 °C they obtained highly crystalline colloidal InSb quantum dots. Unfortunately, the quantum dots were highly polydisperse and their absorption spectrum showed no distinct optical features (Figure 4.2 (a), (b)).

The origin of the high degree of polydispersity of the quantum dots obtained by Tamang *et al.* can be deduced from the X-ray diffraction (XRD) patterns taken at different stages of the synthesis (Figure 4.2 (c)). The patterns indicate that antimony is reduced first under formation of antimony nanocrystals. Only after a minute, indium is incorporated into the antimony nanocrystals and InSb quantum dots are formed. This difference in reduction speed of the indium and antimony precursors severely limits the control over the quantum dot size and shape.

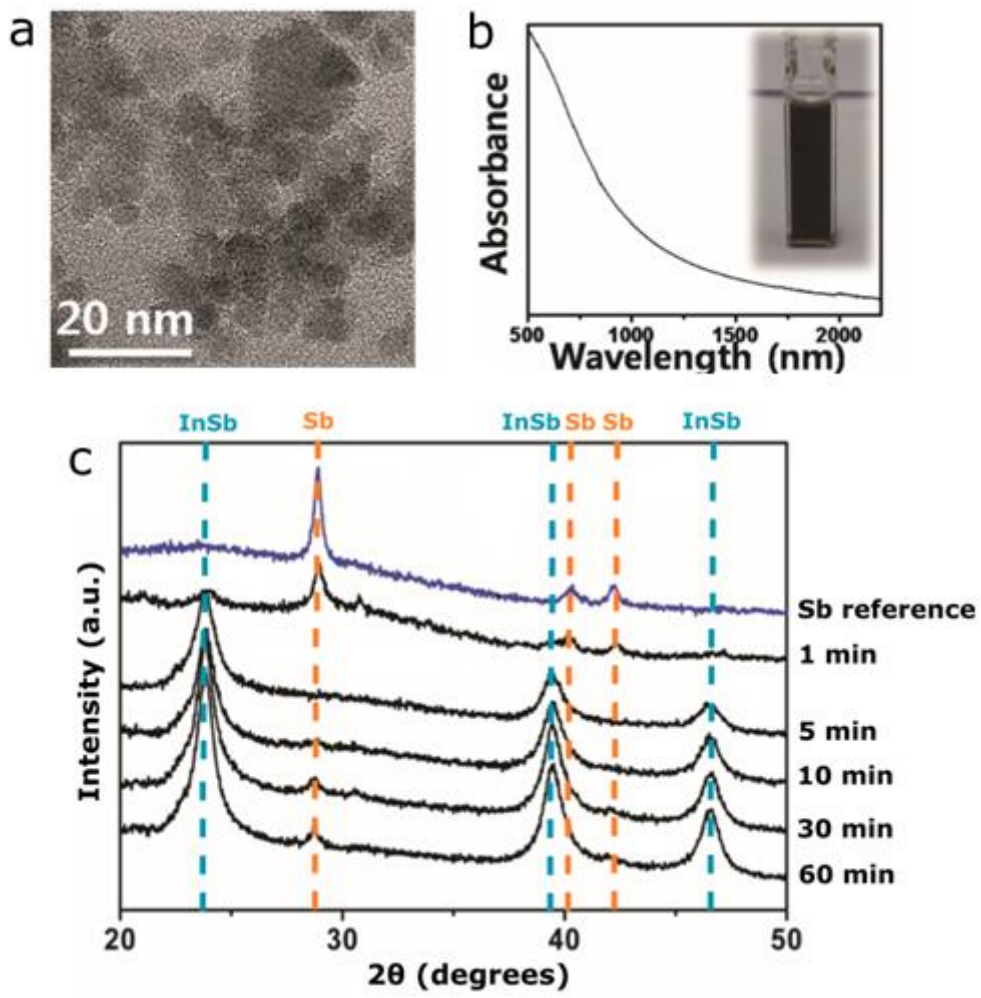

Figure 4.2: Results obtained on the synthesis of colloidal InSb quantum dots as performed by Tamang *et al*.[7] (a) TEM image of the product InSb quantum dots. (b) Featureless absorption spectrum of the product InSb quantum dots. (c) XRD patterns of the reaction products taken at different stages of the synthesis, showing that the particles formed at the initial stages of the synthesis are composed of pure antimony. Adapted from Ref. [7]

This thesis presents a novel preparation method for highly crystalline colloidal InSb quantum dots that relies on the same commercially available precursors ($InCl_3$ and $Sb[NMe_2]_3$) and offers control over the quantum dot size and shape. This striking contrast to the work carried out by Tamang *et al.* is achieved by the use of a single-source precursor containing a weak In·Sb bond. The possibility of the formation of a dative In·Sb bond was proven by Baldwin *et al.*, who characterized the compound $(Me_3SiCH_2)_3In{\cdot}Sb(SiMe_3)_3$ in the solid state using NMR spectroscopy, elemental analysis and single-crystal X-ray analysis.[18] They determined that the In·Sb bond length of this compound was 3.0078(6) Å.

The single-source precursor developed in this thesis is prepared by simply mixing $Sb[NMe_2]_3$ and $InCl_3$ together into a precursor solution prior to the synthesis. Since $InCl_3$ is a strong Lewis acid, and $Sb[NMe_2]_3$ is a weak Lewis base, the two precursor compounds form a weakly bound Lewis adduct *in situ*. This adduct keeps the In and Sb atoms in close proximity. Thereby, it makes the controlled formation of stoichiometric InSb particles more likely. This mechanism is discussed in more detail below.

This section will describe the preparation of the precursor solution, provide evidence supporting the formation of an In·Sb bond and present a spectroscopic analysis of the precursor compound. Finally, a model will be proposed for the formation of the In·Sb Lewis adduct.

4.1.1 Preparation of the precursor solution

The first step in the preparation of the precursor solution is the addition of toluene, oleylamine and $Sb[NMe_2]_3$ to a vial. Upon mixing, the solution turns a bright yellow colour. Subsequently, solid $InCl_3$ is added. Upon mixing and slight heating, $InCl_3$ will be dissolved, yielding a clear and bright yellow solution. The solution remains stable for several weeks. In case the yellow colour fades or some precipitation is observed on the bottom of the vial, slight heating will help to re-obtain the clear and bright yellow solution.

Additional experiments showed that this precursor solution can also be prepared using octylamine, dodecylamine, hexadecylamine and octadecylamine. However, when the secondary amine di-n-octylamine was used, no bright yellow colour was observed and $InCl_3$ could not be dissolved.

Control experiments showed that $InCl_3$ is insoluble in neat toluene, neat oleylamine or neat $Sb[NMe_2]_3$. Therefore, the solvation of $InCl_3$ in a mixture of these three compounds provides a strong evidence for the formation of an In·Sb Lewis adduct.

4.1.2 Spectroscopic analysis of the In·Sb Lewis adduct

In order to determine what compound is present in the precursor solution, ^{1}H and ^{13}C NMR measurements were performed. Due to the low purity of oleylamine, octadecylamine (ODA, ≥99.0% purity) was used to prepare the precursor solution that was analysed using NMR. The results of these experiments can be found in appendix A and are discussed in the next paragraphs.

Both the ^{1}H and ^{13}C NMR spectra show that when $Sb[NMe_2]_3$ is mixed with an equal molar amount of ODA, the resulting solution does not show any peaks that originate from ODA. Instead, we observe peaks that belong to dimethylamine. This result implies that the octadecylamine molecules replace the dimethylamido groups on $Sb[NMe_2]_3$ under the release of dimethylamine. Additional evidence for the substitution of the dimethylamido groups by the amine molecules is the colour change that is observed upon mixing of $Sb[NMe_2]_3$ and the amine.

When more than the equal molar amount of ODA is added to $Sb[NMe_2]_3$, we see that the peaks from ODA become visible in the NMR spectrum. This suggests that only one of the dimethylamido groups of the antimony precursor is fully substituted by the amine molecule. It is not clear if the substitutions of the second and third dimethylamido groups are equilibrium reactions or if the substitution of the second and third groups simply does not occur at all.

The results obtained from NMR spectroscopy are in good agreement with the result obtained from FTIR spectroscopy (Figure 4.3). The reference spectrum that was taken for pure octadecylamine in tetrachloroethylene (TCE) showed that ODA has two absorption features at 3330 and 3390 cm^{-1}, corresponding to the symmetric and asymmetric stretching of the amine group.[19] After mixing ODA with $Sb[NMe_2]_3$, the positions of the peaks originating from ODA redshift to 3300 and 3360 cm^{-1}, respectively.

This observation supports the scenario in which one NMe_2 group is substituted with an ODA molecule. We propose that the redshift of the N-H stretching peaks is caused by the transfer of

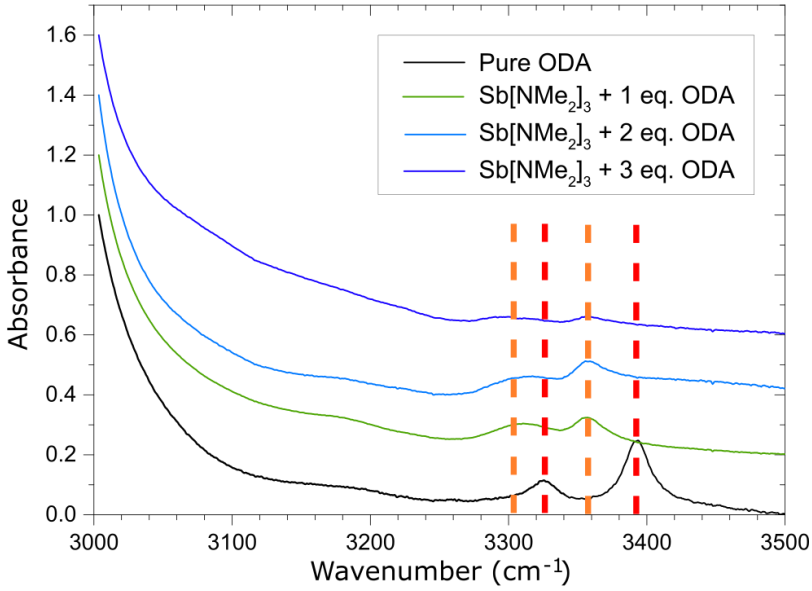

Figure 4.3: FTIR spectra of solutions containing the antimony precursor and increasing amounts of ODA. The reference spectrum of pure ODA indicates that the peaks originating from ODA shift to lower frequencies upon binding to $Sb[NMe_2]_3$.

electron density from the nitrogen atom to the antimony atom upon the binding of ODA to $Sb[NMe_2]_3$. This weakens the N-H bond and therefore causes its stretching vibrations to redshift. The addition of more than the equal molar amount of ODA does not have any consequences for the positions of the ODA signals.

The combination of the ^{1}H NMR, ^{13}C NMR and FT-IR results provides strong evidence for the substitution of one of the dimethylamido groups of the antimony precursor with an ODA molecule. We find that only this substituted antimony precursor can react with $InCl_3$ under the formation of the Lewis adduct.

4.1.3 Model for the formation of the In·Sb Lewis adduct

From the results presented in the previous section, we propose the following mechanism for the formation of the In·Sb adduct:

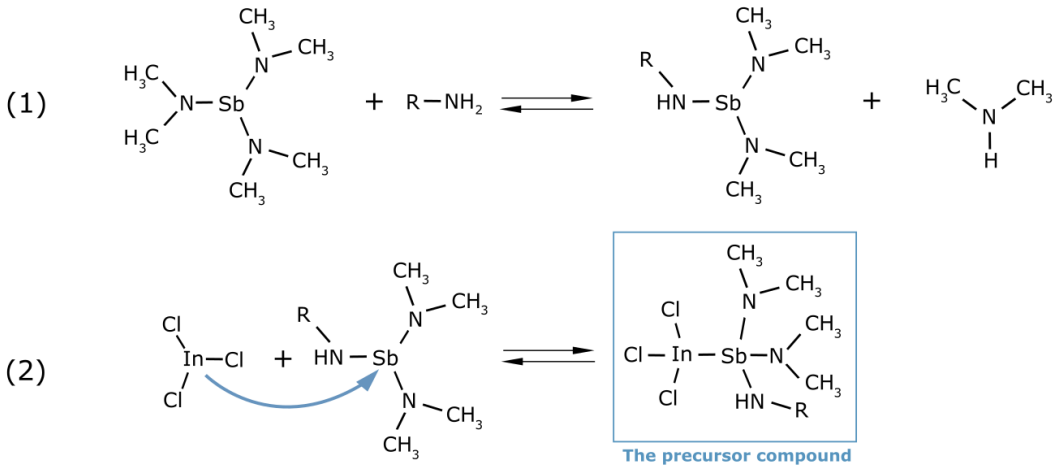

Figure 4.4 Schematic representation of the formation of the single-source precursor compound

We suggest that the formation of the In·Sb Lewis adduct can only take place with the substituted antimony precursor due to steric reasons. When the three dimethylamido groups are bound to the antimony atom, the compound is so bulky that the $InCl_3$ molecule will be unable to approach it. Substitution of one dimethylamido group with a primary amine, however, generates enough space for the $InCl_3$ to bind to the antimony precursor.

We found that the stability of the precursor compound can be extended from several weeks to several months by evaporating a part of the solution under vacuum and replacing it with neat toluene. We propose that this is a result of the evaporation of dimethylamine, which prevents the backward reaction in Figure 4.4 (1) and thereby promotes the forward reaction in Figure 4.4 (2).

4.2 Synthesis of colloidal InSb quantum dots

The precursor solution described in section 4.1 can successfully be used to synthesize crystalline and stoichiometric colloidal InSb quantum dots. This section will discuss the optimized preparation method, present an investigation of the parameter space, propose a reaction mechanism and describe the different reaction products that are obtained.

4.2.1 Strategy

As discussed in section 4.1, the nucleation and growth of InSb quantum dots is thought to take place through In^0 and Sb^0 intermediates.[4] Therefore, existing synthesis procedures employ strong reducing agents to reduce the In and Sb precursors to their zero-valence state. The first step in the new preparation method described in this section is the injection of the strong reducing agent into a hot weakly coordinating solvent. Shortly afterwards, the precursor solution containing In·Sb Lewis adducts is injected into this strongly reducing solvent. This way, the reduction step of the In·Sb Lewis adduct should be very fast. If the reduction rate of the In·Sb Lewis adduct is faster than its dissociation rate, the precursor atoms form InSb units rather than independent In^0 and Sb^0 atoms. The nucleation and growth of InSb quantum dots should thus be kinetically favoured over that of In and Sb metallic nanocrystals. This allows us to retain control over the quantum dot size and shape.

4.2.2 The optimized preparation method

Despite its relatively low purity (70%), oleylamine is preferred as reaction solvent because it is a liquid at room temperature and has a high boiling point. In the optimized preparation method, oleylamine is loaded into a round-bottom flask that is equipped with a thermometer. In order to prevent the release of large volumes of vapour into the glove box during the synthesis, the flask is topped with a vigreux column. The oleylamine is heated to 240 °C. Upon reaching this temperature, the reducing agent (lithium triethylborohydride, 1 M in DOE) is injected. The temperature drops and the solvent turns orange. The temperature is raised back to 240 °C and kept steady by adjusting the height of the heating plate. After waiting for 10 minutes, the precursor solution is injected. The colour of the solution changes from orange to brown and black within thirty seconds. The mixture is allowed to react for 4 minutes at 240 °C and is subsequently quenched by transferral to a cold vial containing toluene.

A TEM image of the reaction products obtained using the optimized preparation method is given in Figure 4.6. The quantum dots have a binomial size distribution - there is a fraction of quantum dots with a diameter of 5.6 nm ± 14% and a fraction of quantum dots with a diameter of 14.9 nm ± 6.4%. The particles are composed of 47% In and 53% Sb.

In the process of optimizing the preparation method, many parameters were varied. In the next subchapter we will discuss the parameters that were varied and the effects we observed on the outcome of the reaction.

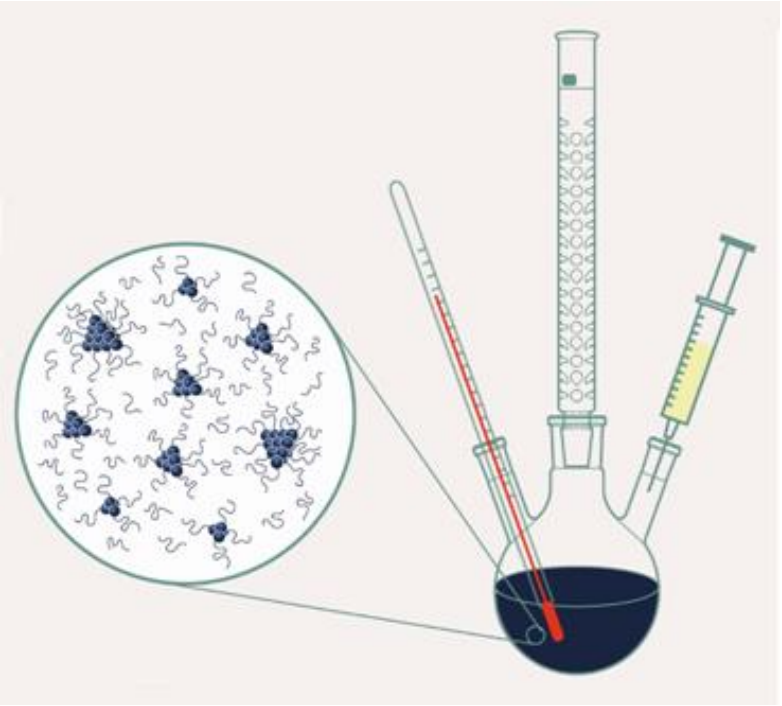

Figure 4.5: Schematic representation of the synthesis set-up depicting the roundbottom flask containing the black reaction mixture obtained after the precursor injection, the vigreux, the thermometer and a syringe which contained the precursor solution. The zoom-in shows small InSb clusters coordinated by oleylamine.

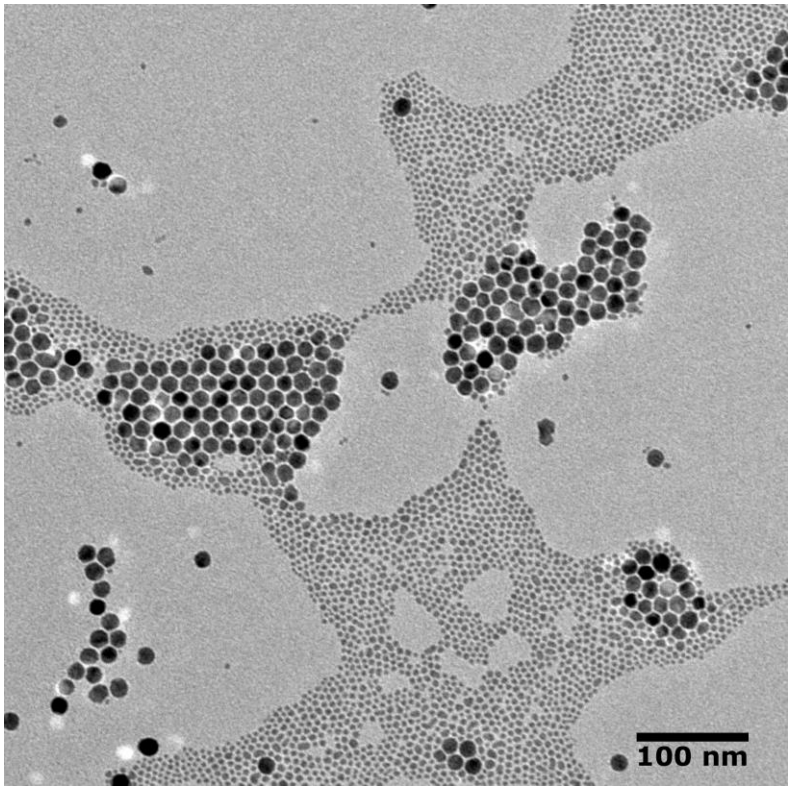

Figure 4.6: The colloidal InSb quantum dots obtained from the optimized preparation method after colloidal stabilization and purification.

4.2.3 Investigation of the parameter space

As mentioned above, many synthesis were carried out in which some of the parameters were varied. Whereas the variation of some parameters did not seem to have to any significant effect, other parameters were found to play a crucial role in the outcome of the reaction. In this section we will discuss the significance of the following parameters: reaction solvent, reaction time, concentration, reaction flask, reaction temperature, amount of reducing agent and time interval between the injection of the reducing agent and the injection of the precursor solution. Our interpretation of the significance of the parameters is presented in section 4.2.4.

However, an investigation of the parameter space makes no sense when the experiment is not reproducible. In order to gain a sense for the reproducibility of the synthesis, three syntheses were carried out in which all reaction parameters were kept constant. The triplicate reactions displayed indistinguishable behaviour and their temperature graphs were very similar. The temperature graphs, TEM images and additional information on these three triplicate reactions can be found in Appendix B. From these experiments, it was concluded that the reproducibility of the synthesis was sufficiently high for an investigation of the parameter space to be sensible.

In order to judge the effects of the parameters on the outcome of the reaction, we had to make a clear distinction between “good” and “bad” samples. We defined “good” samples as samples that contain crystalline and stoichiometric quantum dots with regular shapes. Moreover, good samples have narrow quantum dot size dispersions, ideally of 10% or narrower. In case the product quantum dots have a binomial size distribution, this criterium holds for the separate populations. Samples that we categorized as “bad” are In- or Sb-rich, have irregular shapes and/or broad size dispersions. Additionally, bad samples may contain a lot of by-products. The three types of by-products that were regularly encountered in our reaction mixtures are depicted in Figure 4.7.

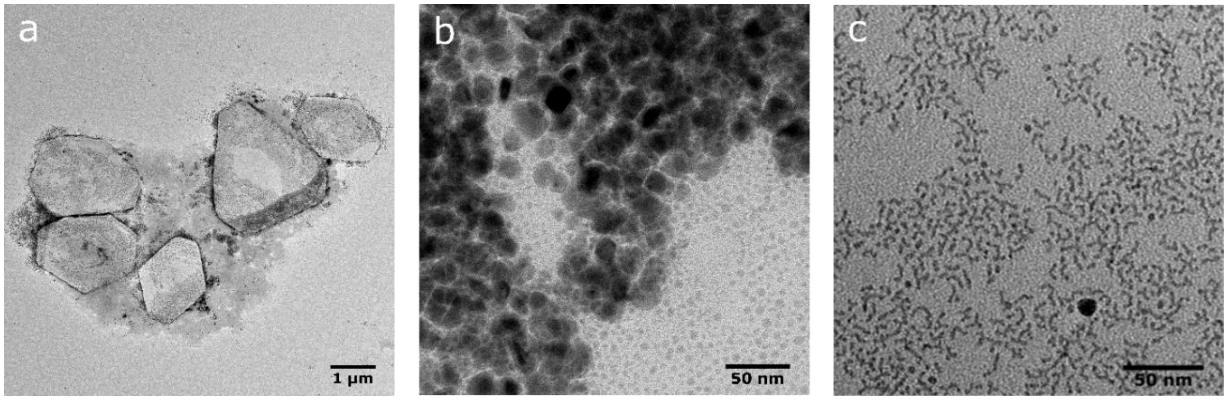

Figure 4.7: The three by-products that were regularly encountered in the reaction mixtures. a) Organic sheets, (b) antimony-rich particles and (c) nanoworms.

The first by-product that we found in our reaction mixtures are sheets with geometrical shapes. The sheets are typically hundreds of nanometers to several micrometers in lateral size. Judging from the low contrast of these sheets in TEM images, they are likely made of an organic material. Possibly, they are formed through the ordering of surfactant molecules into two-dimensional assemblies. The second by-product that we encounter are irregularly shaped antimony-rich particles that are typically 20 to 50 nm in size. As discussed below, the formation of these particles is likely caused by an imbalance in the reaction kinetics. Finally, we observed nanoworms that have a varying length and a width of 1 to 2 nm. Since they are composed of InSb, they are most likely formed through the attachment of small InSb clusters.

During our investigation of the parameter space, we found that one of the parameters that did not observably affect the outcome of the reaction was the type of primary alkylamine used as coordinating solvent. Several syntheses were carried out in which oleylamine was replaced by the primary alkylamines dodecylamine, hexadecylamine and octadecylamine. The reaction products did not show any significant deviation from the products obtained using oleylamine.

In order to assess the influence of the reaction time on the reaction products, aliquots were taken from the crude reaction mixture at different stages of the synthesis (t = 1 minute, 4 minutes and 6 minutes). Although the results regarding the effect of the reaction time on the reaction products were inconclusive, we found that the effect was very limited.

The concentration of the precursors in the reaction medium was varied by changing the precursor-to-solvent ratio from the usual concentration (c_0) to $0.67c_0$ and $2c_0$. No significant effects were observed in the reaction products within this concentration range.

Two different types of reaction flasks were used for the synthesis of colloidal InSb quantum dots: a 20 mL vial and a 50 mL round-bottom flask. High quality quantum dots could be obtained using either of the flasks. However, the reaction kinetics appear to be significantly different in the two types of containers. We observed that when using the vial, the colour change of the reaction mixture upon injection of the precursor solution is faster than when the round-bottom flask is used.

A variable that was found to have a crucial effect on the reaction outcome is the reaction temperature. Although a typical synthesis was carried out at a reaction temperature of 240 °C, we found that the reaction temperature can be varied between 230 and 260 °C without any observable consequences for the reaction products. However, when the reaction temperature is decreased below 230 °C, the product nanocrystals are no longer stoichiometric. A synthesis carried out at 210 °C yielded In-rich nanocrystals with an elemental composition of 80% In and 20% Sb. The majority of the antimony ended up in large and irregularly shaped particles that were composed of 15% In and 85% Sb. A representative TEM image of these reaction products is presented in Appendix C.

We found that the size of the product quantum dots can be tuned by the amount of reducing agent that is injected during the synthesis. A larger amount of reducing agent results in smaller quantum dots, whereas using a smaller amount of reducing agent yields larger quantum dots. TEM images and size diagrams of quantum dots obtained using different amounts of reducing agent are presented in Appendix D. Liu *et al.* also reported on the influence of the amount of reducing agent on the InSb quantum dot size.[4] In their case, however, a larger amount of reducing agent led to larger InSb quantum dots.

Finally, we found that the time interval between injection of the reducing agent and the injection of the precursor solution is a very important variable. When this time interval was extended from roughly 2 minutes to 5 or 10 minutes, significantly improved reaction products were obtained. The product InSb quantum dots had a narrower size dispersion and less by-products were formed. TEM images of quantum dots prepared using different time intervals are presented in Appendix E.

4.2.4 Proposed reaction mechanism

In this section, the effects of the variation of the reaction parameters discussed above are interpreted. Combined with knowledge obtained from the literature and our own observations, they are used to propose a reaction mechanism for the formation of InSb quantum dots.

Liu *et al.* proposed that InSb quantum dots are formed through In^0 and Sb^0 intermediates.[4] This idea is based on their observation that the presence of a strong reducing agent is crucial for the formation of InSb quantum dots. In the absence of the reducing agent, no InSb quantum dots but a black amorphous precipitate was obtained. We, too, find that the reducing agent plays a crucial role in the InSb quantum dot synthesis. A synthesis that was performed without the strong reducing agent yielded metallic Sb cubes (Figure 4.8). This result indicates that the Sb precursor is more readily reduced than the In precursor. Also the XRD patterns presented by Tamang *et al.*[7] (Figure 4.2), which show that metallic Sb particles are formed in the first stages of the synthesis, support this statement.

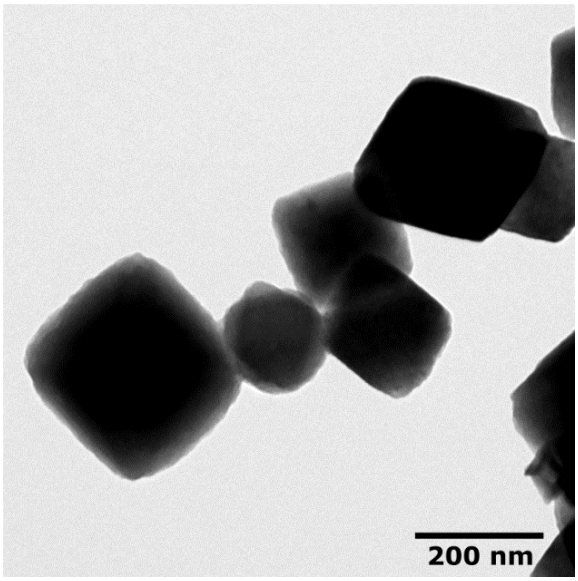

Figure 4.8: When the synthesis is carried out without the addition of the reducing agent, metallic Sb cubes are obtained.

The difficulty in the synthesis of InSb quantum dots lies mostly in finding the right kinetic balance between a number of competing processes. The classical nucleation and growth theory states that the first step in nanocrystal nucleation and growth is the formation of monomers.[13] For semiconductor nanocrystals, these monomers are usually cation-anion pairs. However, since In and Sb both have an oxidation state of +3 in the precursor compounds $InCl_3$ and $Sb[NMe_2]_3$, this cation-anion pair will not form in the case of InSb. Instead, the monomers are the In^0 and Sb^0 atoms that form upon reduction of the precursor compounds. Because the In^0 and Sb^0 atoms are completely independent of each other, a slight imbalance in their reduction kinetics would cause the two elements to separate, leading to the formation of single composition In or Sb metallic particles instead of InSb nanocrystals. This is problematic since, as discussed above, Sb is more readily reduced than In.

In existing literature on the colloidal synthesis of InSb quantum dots, several methods are employed to influence the reaction kinetics. A widely used method is to make use of a strong reducing agent that speeds up the reduction of both the In and Sb precursors and thereby reduces the difference between their reduction speeds. As discussed above, the use of a reducing agent is in fact an indispensable step in the synthesis of InSb quantum dots, and abandoning it indeed leads to the formation of metallic Sb (Figure 4.8). However, the influence of the reducing agent may still be insufficient. The procedure by Tamang *et al.*, for example, employs a strong reducing agent, but from the XRD diffraction patterns taken of the reaction mixture it can be deduced that Sb still reduces before In and forms metallic Sb particles.[7] Liu *et al.* managed to prevent the separation of

In and Sb by synthesizing the precursor compound $Sb[N(Si(Me)_3)_2]_3$, which is less readily reduced than commercially available precursors for Sb.[4] Similarly, Yarema *et al.* synthesized the precursor compound $In[N(Si(Me)_3)_2]_3$, which is more readily reduced than available precursors for In.[6] Yarema *et al*. needed to add a large excess of this indium precursor in order to obtain stoichiometric InSb quantum dots.

In order to kinetically favour the formation of InSb nanocrystals over single composition In or Sb metallic particles, we created a single source precursor *in situ* that contains a weakly bound In·Sb Lewis adduct. The In·Sb bond makes that In and Sb are no longer independent and therefore greatly lowers the chance that they separate to form In or Sb metallic particles. In the synthesis of InSb quantum dots using this adduct, the two competing processes are (1) the reduction of the In·Sb Lewis adduct under the formation of a "InSb" molecular unit and (2) the dissociation of the Lewis adduct. In the new preparation method presented in this thesis, the precursor solution containing the In·Sb Lewis adducts is injected into a solution in which the strong reducing agent is already present. This results in a very fast reduction step. Thereby, the formation of "InSb" molecular units is favoured over the dissociation of the adduct. Through nucleation and growth of these "InSb" monomers, we end up with stoichiometric InSb quantum dots. The improvement of our results (Figure 4.6) over those obtained by Tamang *et al.* (Figure 4.2), who used the same precursor compounds but didn't form the Lewis adduct, can be regarded as an evidence for the formation of this adduct and its successful use.

The previous section discussed how the reaction temperature was found to play a crucial role in the synthesis of colloidal InSb quantum dots. When the reaction temperature is decreased below 210 °C, the product quantum dots are no longer stoichiometric. Instead, the synthesis yielded In-rich nanocrystals with an elemental composition of 80% In and 20% Sb and irregularly shaped particles that were composed of 15% In and 85% Sb. This result suggests that the decrease of the reaction temperature below 210 °C slows down the reduction kinetics to such an extent that the dissociation rate of the adduct is faster than its reduction rate. The dissociates of the adduct makes In and Sb completely independent once again and therefore they are easily separated from each other. Reaction temperatures between 240 and 260 °C, on the contrary, yield stoichiometric nanocrystals. At these temperatures, the reduction kinetics are faster than the dissociation kinetics. The "InSb" molecular units that are formed upon reduction of the adduct act as monomers in the quantum dot nucleation and growth processes. Therefore, the quantum dots obtained through these processes are stoichiometric.

We believe that the formation of InSb quantum dots is extremely fast. We observed that, in the first 10-30 seconds of the reaction, the colour of the reaction mixture changes from orange to brown and finally black. In order to investigate what happens in the reaction solution at that moment, we took samples from the reaction mixture within the first 10 seconds of the reaction. These aliquots typically had an orange to brown colour (Figure 4.9 (a)). Interestingly, we found that such aliquots taken from three different syntheses had identical absorption spectra with peaks at ~370 nm (Figure 4.9 (b)). These absorption must originate from very small InSb clusters. For comparison, Crisp *et al.* observed absorption peaks at 650 nm for their 1 nm-sized InSb clusters.[8] Using the density of bulk InSb, we estimate that quantum dots of 1 nm in diameter consist of roughly 30 atoms. Since the absorption measurements indicate that our clusters must be considerably smaller than those made by Crisp *et al.*, they may be composed of only a few, or even a single, "InSb" molecular unit(s).

In the previous section, we claimed that the size of the product quantum dots can be tuned by the amount of reducing agent that is injected during the synthesis. We found that the injection of a larger amount of reducing agent yielded smaller quantum dots, whereas the injection of a smaller amount of reducing agent resulted in larger quantum dots. This effect can be explained in the

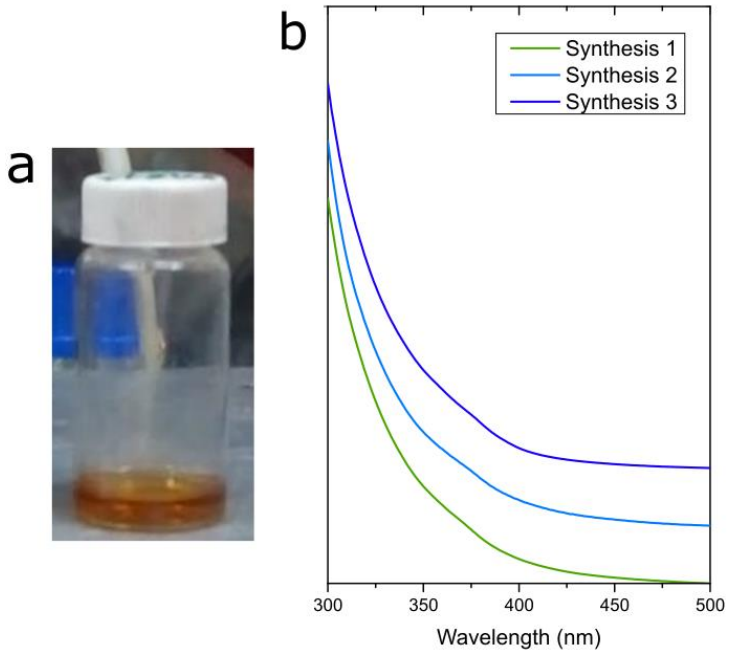

Figure 4.9 The clusters that are formed within the first 10 seconds of the reaction. (a) Picture of the aliquot taken within the first 10 seconds of the reaction. The solution has an orange to brown colour. (b) Absorption spectra of such aliquots that were taken from three different syntheses. All aliquots exhibit an identical absorption peak at ~370 nm.

following way. When the amount of reducing agent is increased, there will be a faster and more complete reduction of the In and Sb precursors. Therefore, in the instant after the injection of the precursor solution, there will be a larger pool of In^0 and Sb^0 available. This leads to the formation of a larger number of nuclei. Because the total number of In and Sb atoms participating in the synthesis remains unchanged, the nuclei will grow into smaller quantum dots.

As discussed in the previous section, aliquots that were taken from the crude reaction mixture at different stages of the synthesis (t = 1 minute, 4 minutes and 6 minutes) showed a limited effect of the reaction time on the quantum dot size. This means that the formation of the InSb quantum dots takes place before the observed time scale and must therefore indeed be very fast. Upon increasing the reaction time, Ostwald ripening should cause the nanoworms observed in our samples (Figure 4.7 (c)) to dissolve and redeposit on the surface of larger particles. However, we observe that the nanoworms remain present in our samples upon increasing the reaction time. We propose that the absence of mass transport is caused by the insolubility of the InSb monomers in the reaction medium. For that reason, Ostwald ripening cannot take place.

From the TEM images that were taken of the crude reaction products, it is clear that we form quantum dots with a binomial size distribution. A possible explanation for this observation is that the quantum dots do not grow through monomer addition. Instead, they grow through coalescence. When the clusters or nanocrystals that coalesce are of comparable dimensions, such growth can produce stepwise size increases.[15] Especially in the synthesis of metallic nanoparticles, the formation of nanocrystals with a binomial size distribution is commonly observed.[20-23] In these reports, the formation of the binomial size distribution is indeed attributed to growth by coalescence.

Based on the fast growth, the apparent insolubility of InSb monomers in the reaction solution and the growth by coalescence, we argue that the formation of InSb quantum dots is a hit-and-stick process. A schematic representation of the hit-and-stick model is given in Figure 4.10. In this model, InSb units (which may be a single molecular unit, clusters or nanocrystals) move freely in solution. When two units collide, they will irreversibly stick to each other. In this way, the formation of bigger units is very fast and the growth is stepwise. Due to the irreversible character of the hit-and-stick process, it is entirely kinetically driven. Therefore, the synthesis of InSb quantum dots is fundamentally very different from the synthesis of quantum dots of other semiconductor materials such as CdTe.

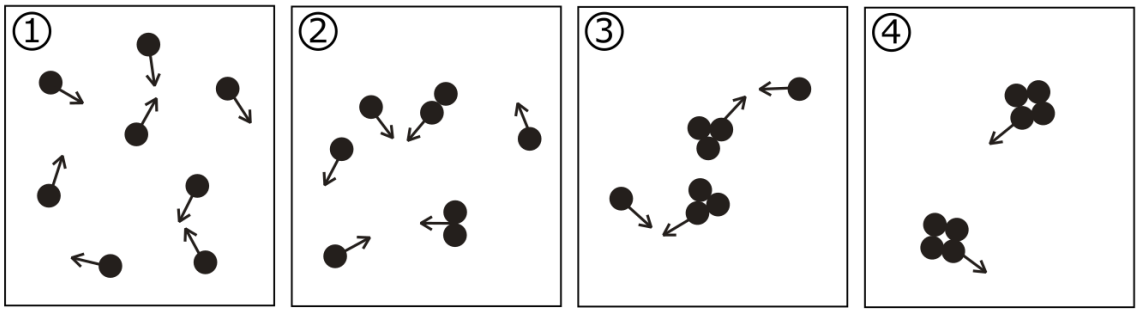

Figure 4.10: Schematic representation of the hit-and-stick model for InSb quantum dot growth.

Although our understanding of the formation of colloidal InSb quantum dots has greatly increased, a number of aspects of the synthesis that are not yet understood. Some examples are the appearance of the orange colour upon injection of the strong reducing agent into oleylamine and the great importance of the time interval between the addition of the reducing agent and the injection of the precursor. A first assumption is that the reducing agent takes part in a side reaction with one or multiple impurities that are present in oleylamine. As a result of these side reactions, the amount of reducing agent decreases and the composition of the solvent changes when the time interval is prolonged. However, control experiments revealed that this orange colour also appears when the reducing agent is injected into amines with high purity at elevated temperatures. Because amines are not susceptible for reduction, the origin of this orange colour remains unclear.

4.2.5 The product quantum dots

Throughout the research presented in this thesis, many syntheses were performed and many varying reaction products were obtained. This section will discuss the sizes, elemental composition and crystal structure of the obtained quantum dots.

Using the novel preparation method presented in this thesis, colloidal InSb quantum dots with sizes ranging from 3.2 to 14.9 nm were prepared (Figure 4.11). No other currently existing preparation method for colloidal InSb quantum dots offers access to such a wide range of quantum dot sizes. Moreover, this thesis is the first report of colloidal InSb quantum dots with diameters exceeding 10 nm. Liu *et al.* reported colloidal InSb quantum dots with sizes ranging from 2.8 nm to 6.3 nm.[4] The quantum dots prepared by Yarema *et al.* ranged from 4.5 to 10 nm[6] and Crisp *et al.* synthesized exclusively 1 nm-sized InSb clusters[8].

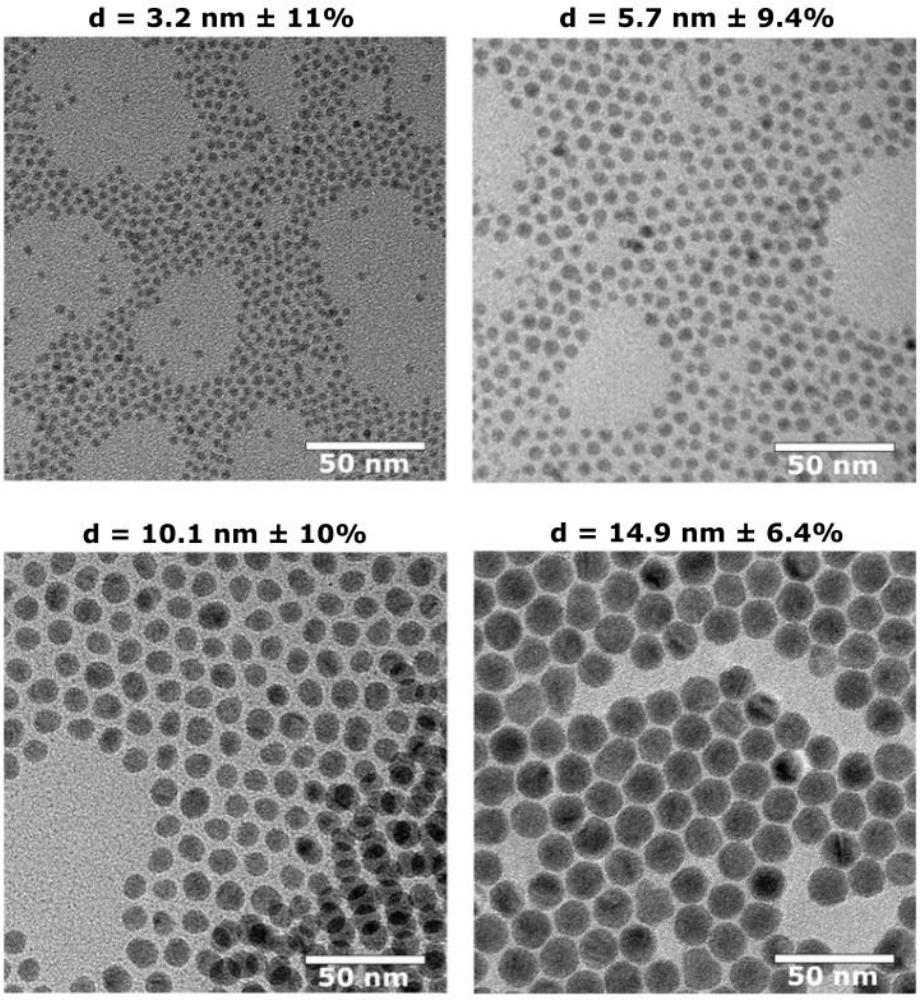

Figure 4.11: Colloidal InSb quantum dots ensembles with sizes ranging from 3.2 to 14.9 nm were obtained using the new synthesis method presented in this thesis.

The elemental composition of the product quantum dots was investigated using energy dispersive X-ray (EDX) spectroscopy. We found that all of the synthesized quantum dots were stoichiometric (composed of 50% In and 50% Sb) regardless of their size. No elements other than In and Sb were detected. EDX maps were taken of a 9 nm-sized batch of quantum dots. These maps, presented in Figure 4.12, show that In and Sb are homogeneously distributed over the quantum dots. Therefore, we conclude that the quantum dots are indeed InSb quantum dots.

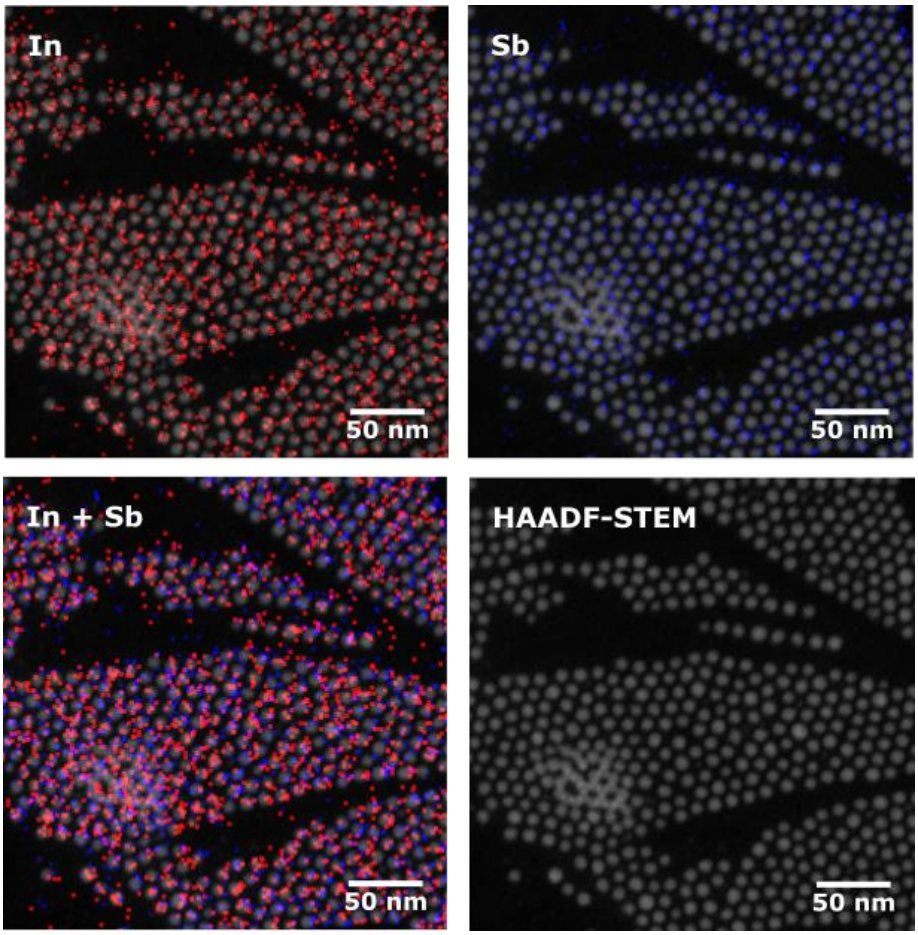

Figure 4.12: EDX map shows the homogeneous distribution of In and Sb over the quantum dots

In order to determine the crystal structure of the quantum dots, bulk electron diffraction (ED) measurements were carried out. Unfortunately, the diffraction patterns of quantum dots with diameters of 10 nm or smaller showed only diffuse rings that did not allow for proper analysis. However, the electron diffraction pattern of the 14.9 nm-sized quantum dots showed well defined rings that we were able to assign to the lattice planes of wurtzite InSb (Figure 4.13 (b)).

The same 14.9 nm-sized quantum dots were analysed using high resolution transmission electron microscopy (HR-TEM). The results that were obtained using this technique are in good agreement with the results obtained using bulk electron diffraction. The major lattice spacings that were observed in the HR-TEM image are 0.37 and 0.40 nm (Figure 4.13 (c)), which correspond to the {100} and {110} lattice planes of wurtzite InSb. The Fourier transform pattern given in Figure 4.13 (d) can be indexed to the [001] axial projection of a wurtzite InSb quantum dot.

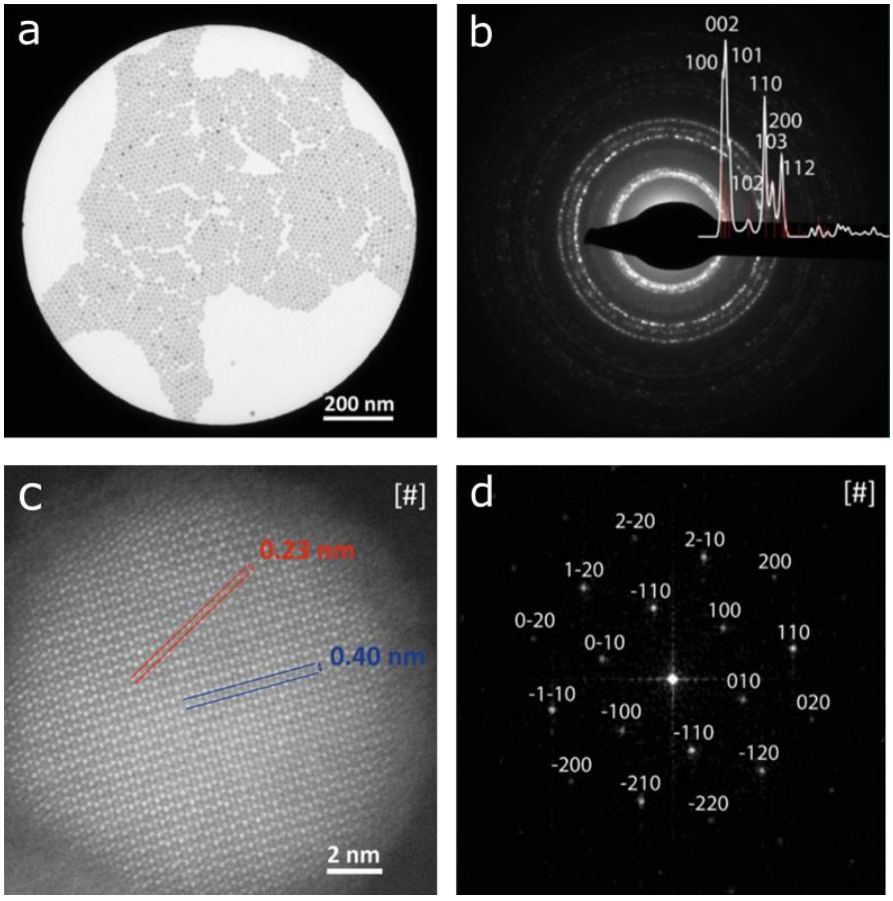

Figure 4.13: Structural analysis of 14.9 nm-sized InSb quantum dots. (a) The area of quantum dots upon which electron diffraction was performed. (b) Selected area electron diffraction pattern of the region shown in (a). The diffraction rings are assigned to wurtzite InSb lattice planes. (c) HR-TEM image in which the major lattice spacings are marked. (d) Fourier transform pattern of the HR-TEM image in which the spots are assigned to wurtzite InSb lattice spacings. Images marked with # are based on measurements carried out by EMAT, Antwerp.

4.3 Post-synthetic treatment: colloidal stabilization, purification and size-selective precipitation

4.3.1. Colloidal stabilization by organic ligands

After completion of the synthesis procedure, the InSb quantum dots are presumably capped with oleylamine ligands. However, we found that the oleylamine-capped InSb quantum dots do not remain colloidal stable throughout the subsequent purification and size-selection steps. We propose that oleylamine is an insufficiently strong ligand because the NH_2 group is a poor electron pair donor that binds only weakly to the In atoms on the quantum dot surface. In order to ensure the colloidal stability of the quantum dots throughout the purification and size-selection, stronger ligands must be added to the reaction solution. Two different ligands were chosen for this purpose. The first one, oleic acid (OA), contains an carboxylic acid head group. The second ligand is dodecanethiol (DDT), which contains a thiol head group. Both the carboxylic acid and thiol head groups are expected to be more powerful electron pair donors and therefore bind more strongly to the In atoms on the quantum dot surface. The molecular structures of oleylamine, oleic acid and dodecanethiol are presented in Figure 4.14.

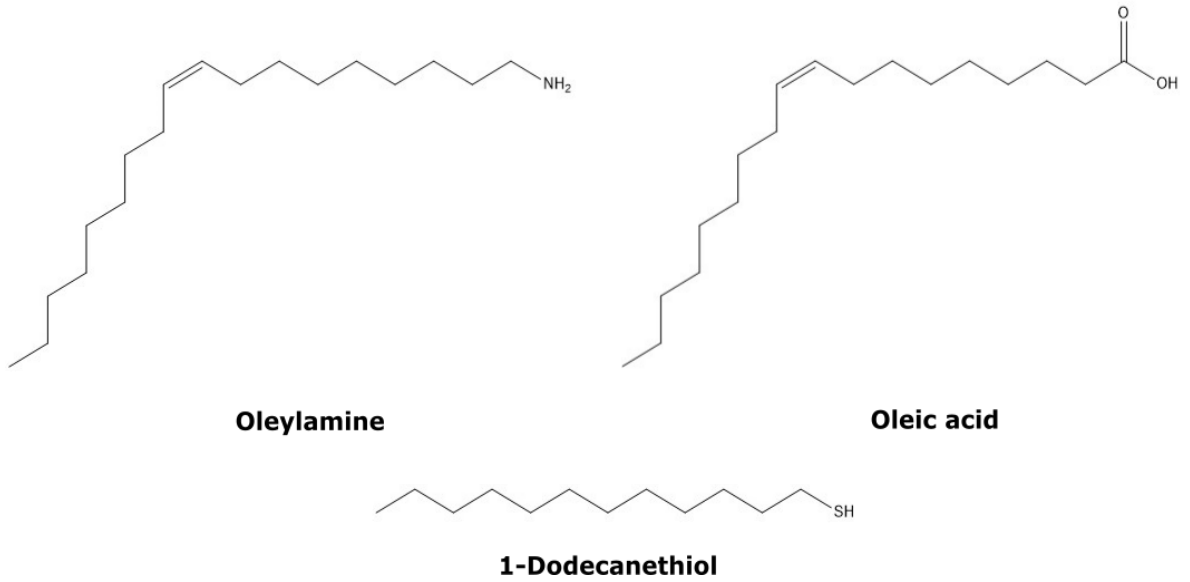

Figure 4.14: The molecular structures of the three ligand molecules employed in this research.

We found two ways to obtain colloidally stable quantum dot dispersions through the addition of stronger ligands. These two different methods will hereafter be referred to as method A and B. In method A, oleic acid is added to the reaction solution 2 minutes after its quenching in toluene. In method B, dodecanethiol is added to the reaction solution 1 minute after its quenching in toluene, and is followed by the addition of oleic acid 3 minutes after its quenching in toluene. In both methods, the reaction solutions have already cooled down to room temperature before the ligands are added. No experiments were performed to investigate the relevance of the moment or sequence of the addition.

The colloidal stability of quantum dots treated according to method A seemed superior to that of quantum dots treated according to method B, since aggregates were observed more often in the latter method. Further evidence for this statement was found upon TEM analysis of the samples. Figure 4.15 shows TEM images of two batches of InSb quantum dots. For each batch, half of the

quantum dots was treated according to method A and half was treated according to method B. The images clearly show that large quantum dots (ø > 8 nm) treated according to method B are prone to fuse, whereas the very same quantum dots do not fuse when they are treated according to method A. This indicates the superior colloidal stability of quantum dots treated according to method A.

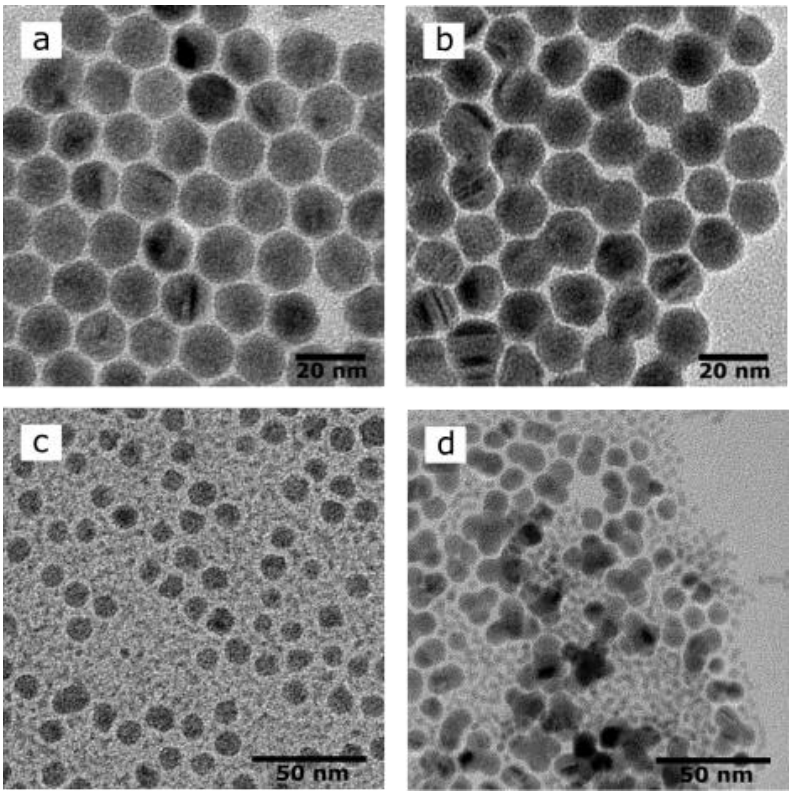

Figure 4.15: The influence of the addition of DDT on the shape of the quantum dots. (a) Quantum dots obtained from batch 1 treated according to method A. (b) Quantum dots obtained from batch 1 treated according to method B. (c) Quantum dots obtained from batch 2 treated according to method A. (d) Quantum dots obtained from batch 2 treated according to method B.

In the samples that were treated according to method A, we often observed particles with interesting shapes (Figure 4.16), such as peanut- and Mickey Mouse-shaped particles. Some samples even contained tetrahedrally shaped particles, which may be interpreted as a starting point for the formation of ABAB lattices.

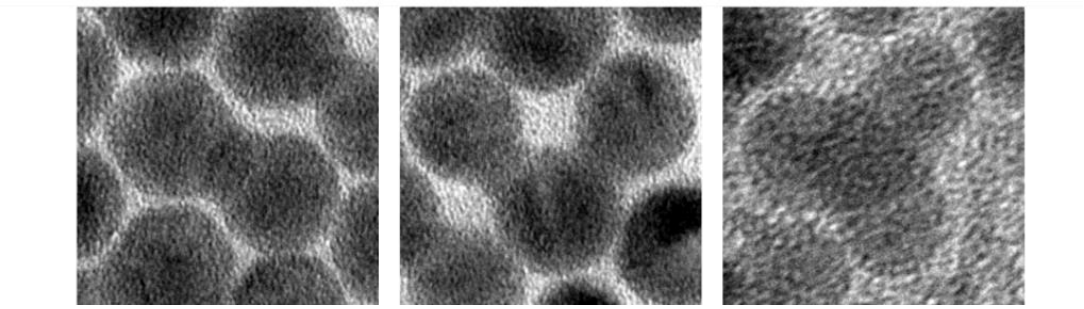

Figure 4.16: Fused quantum dots with interesting shapes in the samples prepared according to method B.

Interestingly, the fused quantum dots do not come in the shape of huge aggregates, but are most frequently observed in the form of dimers and occasionally trimers and tetramers. Possibly, there are one or more specific facets that oleic acid cannot bind to while dodecanethiol can. This idea remains to be investigated. The different results obtained using method A and B suggest the stability of specific facets, and thereby the shape of the nanocrystals, can be tuned by the choice of ligands.

4.3.2 Purification

After the introduction of stronger ligands to the quantum dot surface, the quantum dots were isolated according to the widely used precipitation method. This method involves the addition of a polar solvent to the quantum dot solutions. Since their ligand shell renders the quantum dots highly insoluble in polar solvents, such a solvent is also called an antisolvent. Upon addition of the antisolvent, the quantum dots will lose their colloidal stability and form aggregates. These aggregates are then separated from the solvent by centrifugation and the resulting pellet is redispersed in an apolar solvent with high purity. In order to further lower the amount of contamination, additional washing cycles may be performed.

In order to find out which antisolvent was best suited for the purification of InSb quantum dots, experiments were carried out with a number of commonly used antisolvents, namely acetonitrile, ethanol and a 1:1 butanol:methanol mixture. The butanol:methanol mixture was found to be the most powerful antisolvent of the three. Using this mixture, we were able to precipitate the quantum dots with the lowest amount of antisolvent and the stability of the quantum dots could successfully be re-established after redispersion in toluene. Therefore, the 1:1 butanol:methanol mixture was chosen as the purification antisolvent in the standard synthesis method.

When multiple purification steps were carried out, we observed that the colloidal stability of the quantum dots deteriorated with every step. We propose the following explanation for this observation. We believe the ligands may be dynamically bound to the surface atoms, meaning that the ligands alternate between their bound state and moving free in solution. The equilibrium between bound and free ligands is severely disrupted when the solvent containing the free ligands is removed and replaced by a pure solvent. A new equilibrium will be established in which a lower amount of ligands is attached to the quantum dot surface. Thereby, the quantum dots will slowly lose their colloidal stability.

We tested if the colloidal stability of aggregated quantum dots could be recovered by the attachment of new ligands to the quantum dot surface. This was attempted through the addition of ligands to the aggregated samples and subsequent sonication. In the case of dodecanethiol, this method was indeed successful in recovering stable colloidal quantum dot dispersions. However, in the case of oleic acid, no improvement in colloidal stability was observed. A possible explanation for this observation can be found in a recent article written on $CsPbBr_3$ perovskite nanocrystals.[17] This article describes the reaction of oleic acid with oleylamine in which a proton is transferred from oleic acid to oleylamine. The two molecules then form the ion pair oleylammonium oleate. This ion pair acts as the ligand that stabilizes the InSb quantum dots. Therefore, oleic acid can provide colloidal stabilization when it is added to the crude reaction solution containing oleylamine, but not when it is added to a quantum dot dispersion in toluene, without oleylamine.

4.3.3 Size-selective precipitation

The reaction mixture contains a number of different products with varying composition, size and shape. After the completion of the stabilization and purification steps described above, these

products may be separated from each other using the size-selective precipitation method. This method relies on the same principle as the purification procedure – upon addition of an antisolvent, the colloids are destabilized and can be separated from the solution by centrifugation. However, since van der Waals forces are stronger for bigger particles, bigger particles are more easily destabilized than smaller particles. The size-selective precipitation method makes smart use of this fact by repetitively adding small amounts of antisolvent and separating the biggest particles from the sample (Figure 4.17). In this way, the sample can be divided into multiple fractions that contain different types or sizes of particles.

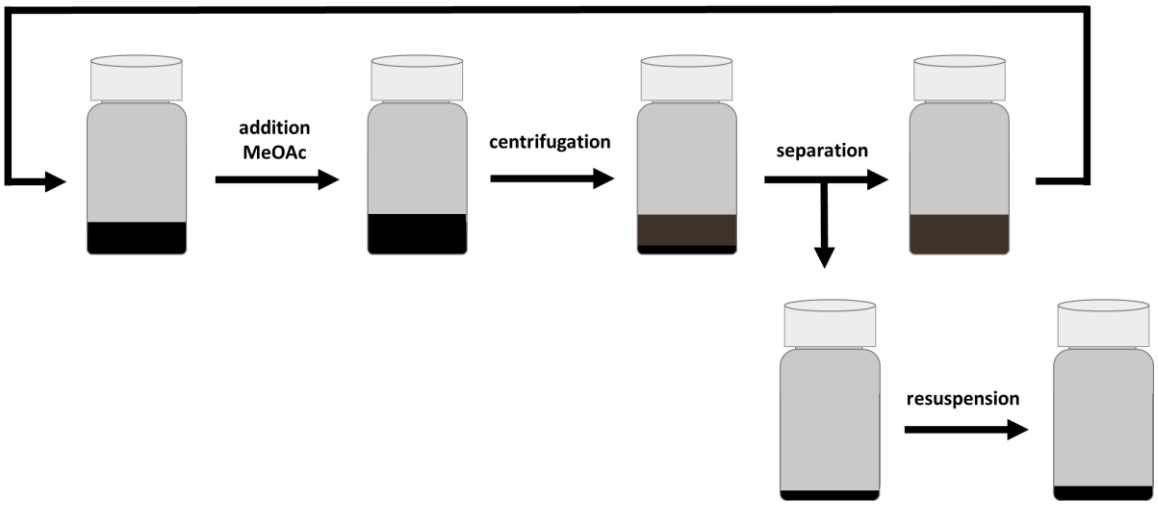

Figure 4.17: Schematic representation of the size-selective precipitation method.

The size-selective precipitation method proved highly suitable for the separation of different products from the reaction mixture. As expected, the large organic sheets with dimensions of several hundreds of nanometers are separated from the quantum dots and nanoworms in the first fractionation step. However, the size-selective precipitation procedure is also successful in more delicate separation tasks. Figure 4.18 shows how the quantum dot ensembles with binomial size distributions can be successfully separated into two fractions of like-sized quantum dots. Even more astonishing is that the procedure can separate the nanoworms from the small, spherical nanocrystals from which they are likely constituted. This can be seen in Figure 4.19. The observation that these two types of particles can be separated from each other is evidence that the nanoworms are formed in solution and not upon drying of the quantum dot solutions on the TEM grids.

Using the size-selective precipitation method, the shape and size polydispersity of the sample is greatly improved. Small polydispersity of the sample is crucial for optical measurements, additional treatments like epitaxial shell growth and application in devices. Therefore, size-selection is an indispensable step within the post-synthetic treatment.

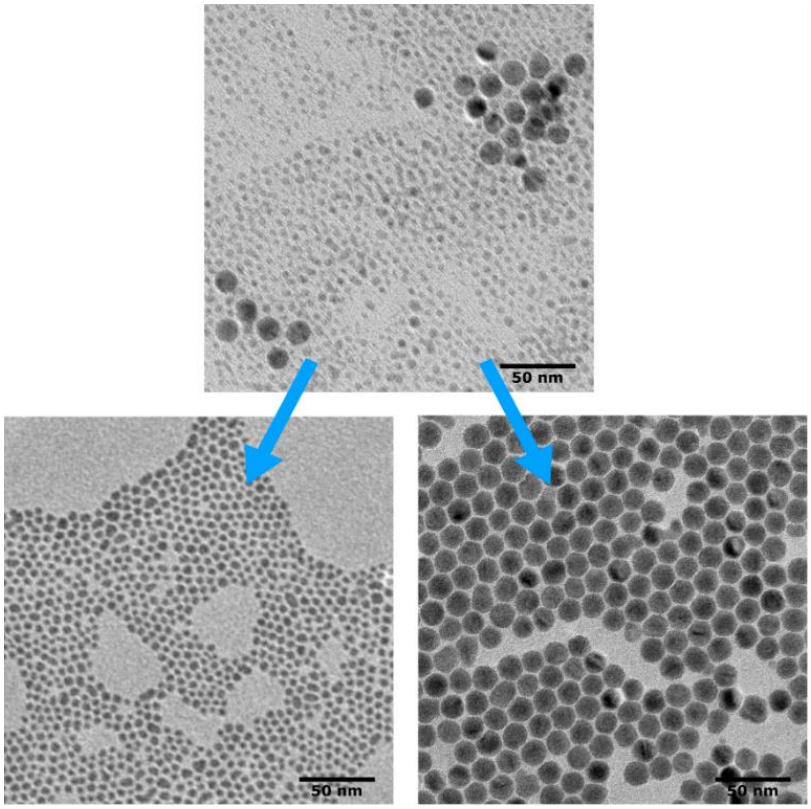

Figure 4.18: A sample containing quantum dots with a binomial size distribution can be separated into two fractions of like-sized quantum dots through size-selective precipitation.

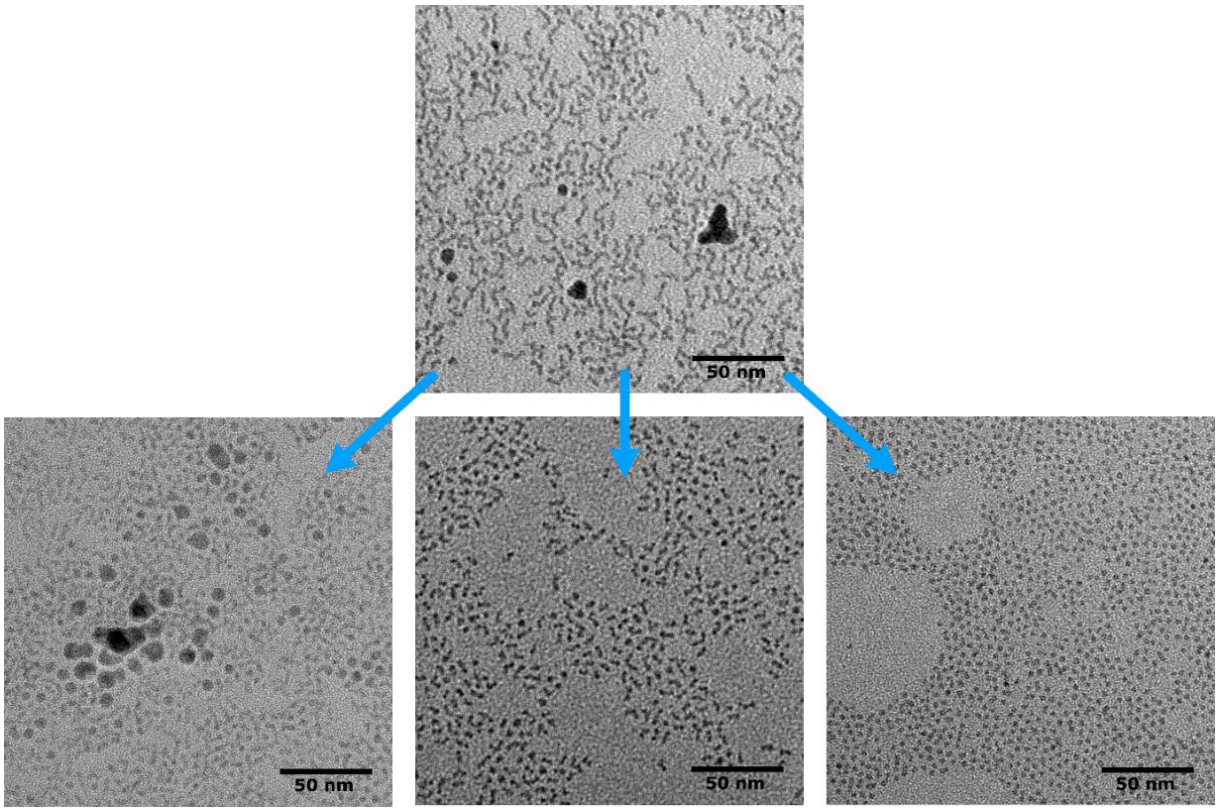

Figure 4.19: A sample containing a mixture of quantum dots and nanoworms can be separated into multiple fractions using size-selective precipitation so that a fraction containing only quantum dots is obtained.

4.4 Investigation of optical properties

Since the exciton Bohr radius of InSb is 60 nm, the colloidal InSb quantum dots described in this thesis experience extremely strong quantum confinement potentials. Consequently, a small deviation in quantum dot size leads to a large deviation in absorption (or emission) wavelength. Therefore, broad optical features are likely inherent to InSb quantum dots in this size regime.

We found that the purified crude reaction products rarely show well-defined optical features, which is likely due to the particle size and shape polydispersity in these ensembles. Therefore, the crude products were separated into fractions according to the size-selective precipitation method described above. The size and shape distributions of the obtained fractions are sufficiently narrow to observe a well-defined peak at the lowest energy absorption edge. This section describes the optical properties that we observed in these fractions using near-infrared absorption spectroscopy, transient absorption spectroscopy and photoluminescence spectroscopy.

4.4.1 Steady-state absorption spectroscopy

Near-infrared absorption spectroscopy is a technique that measures the sample's absorption of light as a function of wavelength in the near-infrared spectral region. Since the electrons in semiconductor quantum dots can be excited from the valence band to the conduction band under the absorption of photons with sufficient energy, the lowest energy absorption edge wavelength is regarded to be equal to the band gap energy of the nanocrystals.

Figure 4.20 (a) shows the absorption spectra that were obtained for quantum dot ensembles with particle sizes ranging from 3.8 to 7.0 nm. We found that the lowest energy absorption edge wavelength varied from 1112 nm (1.11 eV) for 3.8 nm sized quantum dots to 1527 nm (0.81 eV) for 6.9 nm sized quantum dots. These spectra demonstrate the ease with which the band gap energy can be tuned by variation of the quantum dot size.

Unfortunately, the absorption spectra for quantum dots larger than 7 nm could not be obtained. For quantum dots of these sizes, the absorption by the dispersion medium toluene interfered with the measurements. Attempts to transfer the quantum dots to a more appropriate solvent like TCE, which does not absorb in the near-infrared, were unsuccessful. Moreover, we expect that quantum dots with sizes exceeding 10 nm would absorb at wavelengths beyond the measuring range of our spectrophotometer.

In order to investigate size dependence of the band gap of the InSb quantum dots prepared in our work, the band gap energies deduced from Figure 4.20 (a) were plotted together with the quantum dot sizes that were deduced from TEM in Figure 4.20 (b). The sizing curve also includes the experimental results reported by Liu *et al*.[4] for zinc blende InSb quantum dots, and by Yarema *et al.*[6] for wurtzite InSb quantum dots, and theoretical results obtained by Efros and Rosen.[24]

The size-dependent trend observed in our work is in reasonably good agreement with those found by Liu *et al*. and Yarema *et al*. However, the band gaps observed in our work are systematically larger than those reported in the other two papers for similarly sized quantum dots. The reason for this difference remains to be investigated.

The size-dependence of the band gap found from experimental data is much weaker than the size-dependence that was predicted from calculations performed by Efros and Rosen.[24] An explanation offered by Liu *et al.*[4] is the leakage of the exciton wave function into the medium surrounding the quantum dots. This leakage would reduce the quantum confinement energy experienced by the InSb quantum dots and therefore weaken the size-dependence of the band gap energy. However, due to the high dielectric constant of the surrounding medium, the potential offset for such a leakage would be high. Therefore, we do not consider this explanation likely.

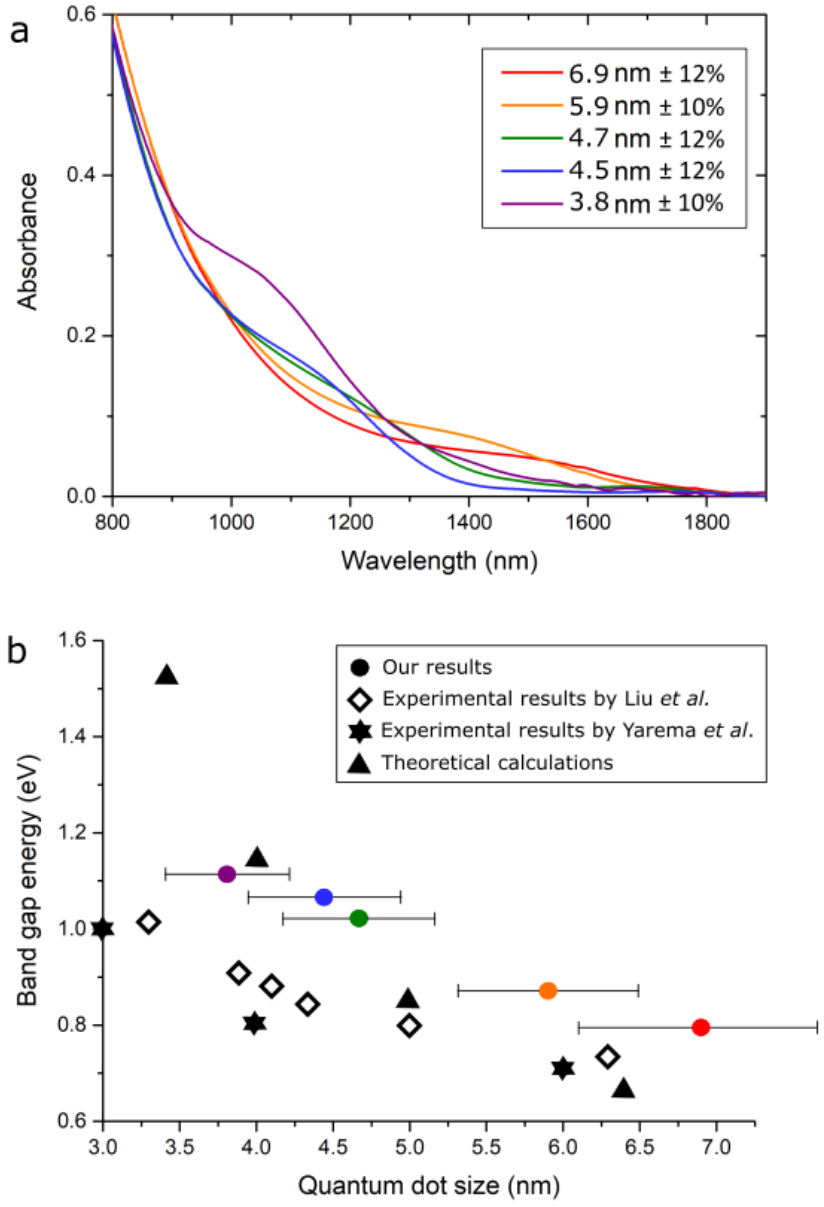

Figure 4.20 (a) Near infrared absorption spectra obtained for quantum dot ensembles with particle sizes ranging from 3.8 to 7.0 nm. The absorption peak wavelength is regarded to be equal to the band gap energy of the particles. (b) A sizing plot depicting our results together with experimental results obtained by Liu *et al.* [4] and Yarema *et al.* [6] and theoretical calculations performed by Efros and Rosen.[24]

The explanation that we propose for the weak size-dependence of the band gap energy is that the parabolic description of the band gap energy as presented in the theory section of this thesis is not the right way to describe this system. The size dependence of the band gap energy of the colloidal InSb quantum dots seems to be mainly determined by the 1/d term instead of the $1/d^2$ term. Such observations have previously been made for copper indium sulfide (CIS)-, PbSe- and PbS quantum dots[25-28] and can be interpreted as evidence that the energy dispersion is mostly linear around the band gap.

4.4.2 Transient absorption spectroscopy

Transient absorption spectroscopy was employed in order to gain insight in the carrier dynamics upon excitation of the colloidal InSb quantum dots. In transient absorption spectroscopy, the quantum dots are promoted to their excited state by means of a pump pulse.[29] After a short delay time another pulse, the probe pulse, is sent through the sample. Absorption spectra are recorded during each pulse. The difference between the ground state absorption and the excited state absorption (ΔA) is then measured for varying delay times and plot in a 2D diagram.

If ΔA for a delay time t is negative, this means that after a time t the quantum dot is still in its excited state. Because the excited state is already populated by charge carriers, it becomes less likely to absorb another photon for a second excitation (Figure 4.21 (a)).[29] This effect is mostly due to the populated electron states, since the electron states have a two-fold degeneracy and the hole states have a six-fold degeneracy. As a result of the occupied electron state, the excited state absorption will be weaker than the ground state absorption and therefore ΔA is negative. A patch in the ΔA spectrum that has a negative value for ΔA is also called a bleach feature. If ΔA for a delay time t is zero, this means that the absorption by the probe pulse is identical to the absorption by the pump pulse. Therefore, the excited state must be vacant after that delay time t. This may be caused by radiative recombination of the exciton or the localization of the electron in a trap state as depicted in Figure 4.21 (b). Alternatively, ΔA may be positive. In this case, the excited quantum dots can be excited for a second time (Figure 4.21 (c)). This is called photoinduced absorption and is usually attributed to trapped charges.[8] Using transient absorption spectroscopy, the decay time of the quantum dots can be determined as the delay time at which ΔA changes from a negative value to zero. Since radiative recombination of the exciton occurs on a nanoscale time range[30], decays that are faster than a nanosecond are usually attributed to the localization of the electrons in trap states.

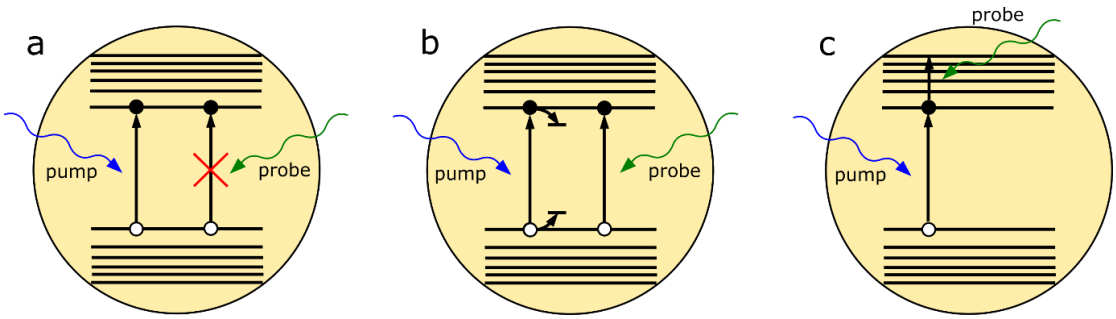

Figure 4.21: The various processes that contribute to the ΔA spectrum. (a) If the quantum dot is still in its excited state after delay time t, ΔA is negative. (b) If the charge carriers are localized at trap states after delay time t, ΔA is zero. (c) If photoinduced absorption takes place, ΔA is positive.

Transient absorption spectra have previously been recorded for colloidal InSb quantum dots by Chang *et al.*[31] and Crisp *et al.*[8] The 4.0 nm-sized InSb quantum dots used by Chang *et al.* showed a bleach at 1400 nm that shifts to longer wavelengths for increasing delay times.[31] Upon further

inspection, they found that this highly unusual redshift becomes larger for larger particles and more distinct at lower temperatures. Chang *et al.* proposed that the redshift is caused by hot exciton cooling through states that arise from energetically close conduction band levels. The decay time determined by Chang *et al*. was 31 ps.

The transient absorption spectrum recorded by Crisp *et al.* for their ~1 nm sized InSb clusters shows two bleach features at 520 and 660 nm.[8] These are the same wavelengths at which peaks are visible in their absorption spectrum. Crisp *et al.* state that the 660 nm feature corresponds to the InSb cluster band gap whereas the 520 nm transition is caused by the spin-orbit split-off band. In contrast to the findings by Chang *et al*., Crisp *et al.* observed no redshift in the bleach features. From the transient absorption plot can be estimated that the decay time of their InSb clusters is 2 to 3 ps.

We performed transient absorption spectroscopy on the quantum dot ensemble presented in Figure 4.22 (a). The ensemble contains InSb quantum dots with a diameter of 6.5 nm ± 9.8% and a small number of nanoworms. The near infrared absorption spectrum of this ensemble (Figure 4.22 (b)) shows an absorption peak around 1450 nm.

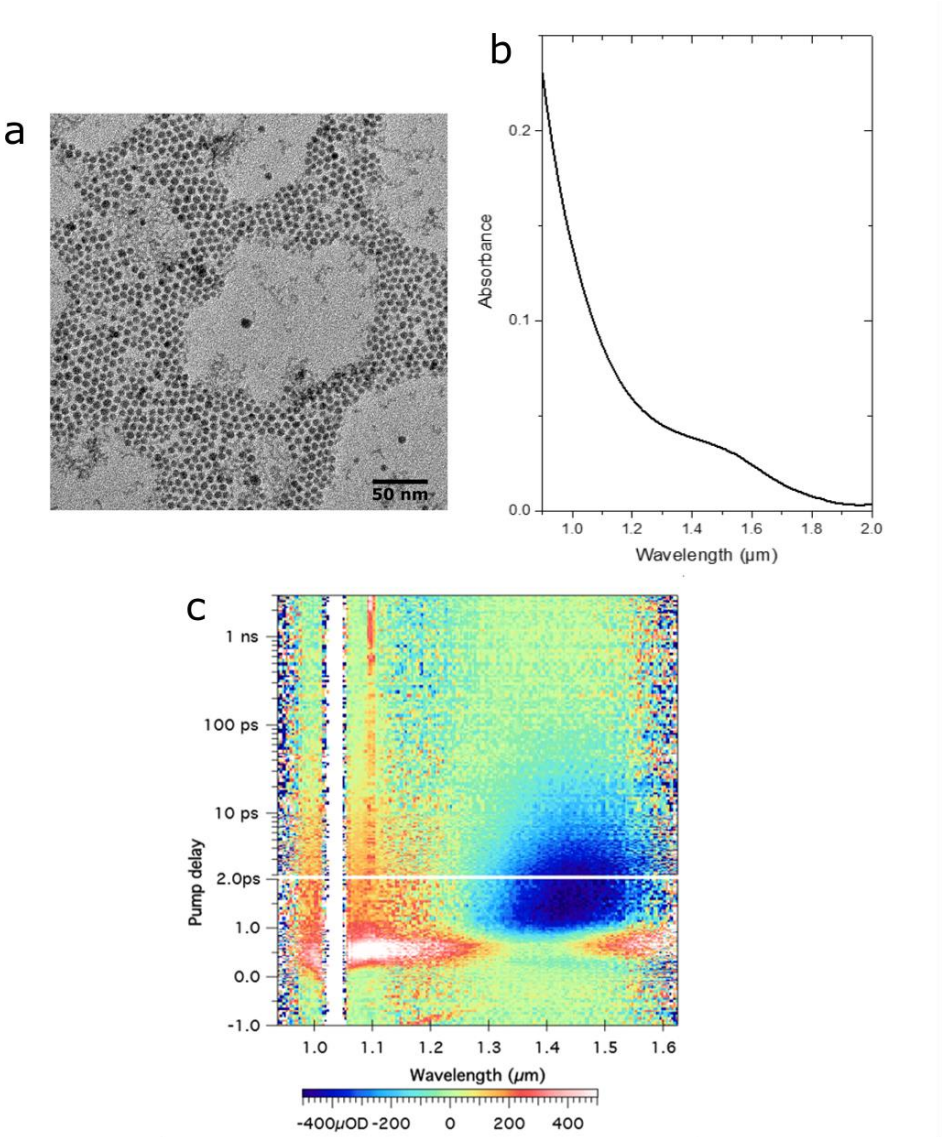

Figure 4.22 (a) The quantum dot ensemble upon which the transient absorption spectroscopy was carried out. (b) The absorption spectrum of this ensemble shows a feature around 1450 nm. (c) The transient absorption spectrum of this ensemble shows a bleach feature around the same wavelength.

The transient absorption spectrum (Figure 4.22 (c)) shows a bleach signal at a spectral position that is identical to that of the lowest energy peak steady-state absorption spectrum. In contrast to the transient absorption spectrum presented by Chang *et al.*[31], our measurements do not show a redshift of the bleach feature with time. The decay time of the bleach feature is roughly 10 ps. This means that up to 10 ps after excitation by the pump probe, the excited state remains populated by electrons so that a second excitation by the probe pulse is unlikely. After 10 ps, the electrons no longer populate the excited state. This suggests that the quantum dots contain defects that cause the localization of the excited electrons at trap states within 10 ps.

4.4.3 Photoluminescence spectroscopy

As described above, the fast decay of the bleach signal that was found in transient absorption measurements indicates that electrons that are excited to the conduction band are quickly localized on defects. Therefore, the decay of the excited state is primarily non-radiative and the photoluminescence of the colloidal InSb quantum dots must be very weak. Nevertheless, photoluminescence measurements performed at room temperature showed a weak and broad signal around 1400 nm (Figure 4.23).

The photoluminescence spectroscopy was carried out on a rather polydisperse quantum dot ensemble. The quantum dot diameter was 5.2 nm ± 19.7%. Due to the broad size distribution, the absorption spectrum obtained for this ensemble was featureless. Nevertheless, using the sizing curve presented in Figure 4.18 (b), the band gap energy of these quantum dots was estimated at 0.94 eV (1320 nm). The broad photoluminescence signal centered around 1400 nm is therefore considerably red-shifted compared to the estimated band gap energy. This can be explained as follows. Because the sample is excited with photons with an energy far exceeding the band gap energy, the absorption of photons becomes a volume-related process. Therefore, larger quantum dots are more likely to absorb photons than smaller photons. As a result, the photoluminescence is dominated by the larger quantum dots, causing photoluminescence at longer wavelengths than expected.

The photoluminescence of the same sample of quantum dots was measured again at a temperature of 4 K. At this temperature, the trapping of charge carriers on point defects is less likely to occur. This is due to the limited thermal energy of the semiconductor atoms, which makes the material unable to reorganize in order to accommodate the localized charge. Therefore, radiative decay is promoted and the photoluminescence intensities increase.

Figure 4.23 presents the photoluminescence graphs obtained at the two different temperatures. In comparison to the photoluminescence signal obtained at room temperature, the photoluminescence signal obtained at 4 K is blueshifted and has a smaller full width half maximum (FWHM).

The blueshift can be explained by the temperature-dependence of the band gap energy, which is common to III-V and II-VI semiconductors.[32-34] The temperature-dependence of the InSb band gap was demonstrated and measured by Littler *et al.*[35] in 1985. They showed that upon decreasing the temperature from 300 K to 4 K, the InSb band gap energy increased by 0.07 eV, going from 0.17 eV to 0.24 eV. From our work we deduce that, under similar conditions, the InSb quantum dot photoluminescence peak position also increased by 0.07 eV, going from 0.89 eV (1400 nm) to 0.96 eV (1295 nm).

The decrease of the FWHM of the photoluminescence signal from 275 meV to 120 meV can be explained by the reduced density of phonon states at 4 K. As a result, the electron-phonon coupling

is much weaker than at room temperature and the homogeneous linewidth is narrow. Therefore, the FWHM observed at 4 K is directly proportional to the size dispersion of the quantum dots. Considering the broad size dispersion of the quantum dots mentioned above, the FWHM of the signal obtained at 4 K is surprisingly narrow. Possibly, only a certain fraction of the quantum dots in the ensemble contributes to the photoluminescence.

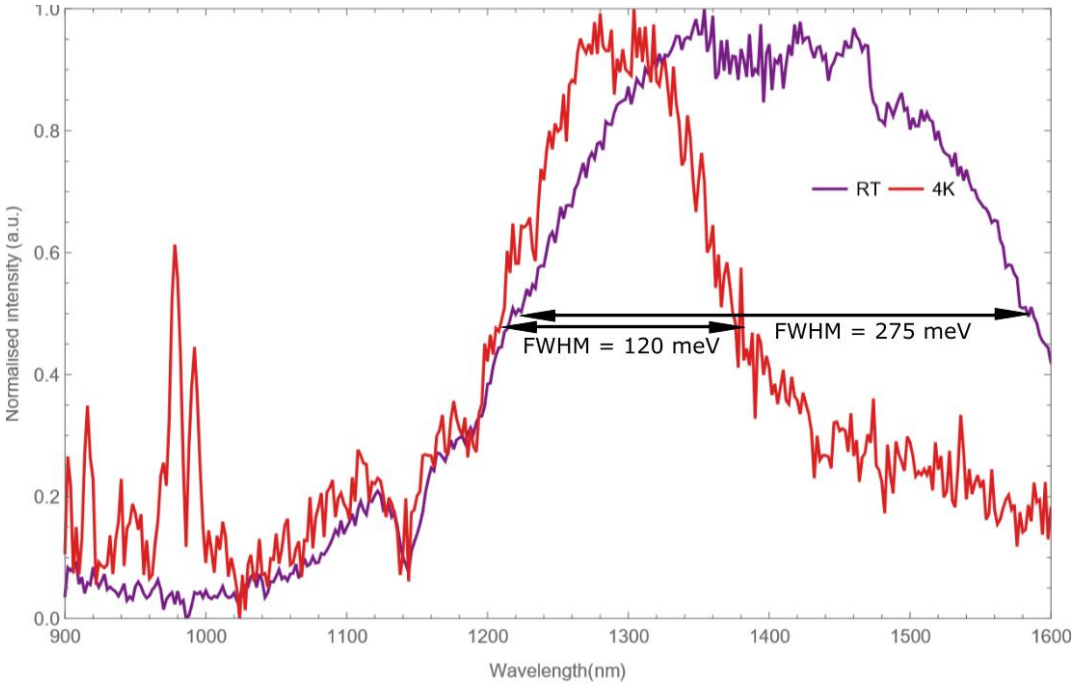

Figure 4.23: Normalized photoluminescence spectra obtained from quantum dots with a diameter of 5.2 nm ± 19.7% using an excitation wavelength of 600 nm. The purple curve was measured at room temperature (RT) and is an average of 3 scans. The red curve was measured at a temperature of 4 K and is an average of 6 scans. Arrows indicate the full width half maximum (FWHM) of the peak.

Even at 4 K, the photoluminescence quantum yield of colloidal InSb quantum dots remains low. Another strategy to promote the radiative recombination of the exciton is the passivation of the dangling orbitals on the quantum dot surface through overgrowth with a heteroepitaxial shell of a suitable material.

Chapter 5: Conclusions and outlook

We have developed a novel method for the synthesis of highly crystalline colloidal InSb quantum dots using only commercially available precursors. We created a single-source precursor *in situ* by mixing $InCl_3$, which is a strong Lewis acid, with $Sb[NMe_2]_3$, which is a weak Lewis base. The molecular structure of the resulting In·Sb Lewis adduct was elucidated using NMR and FTIR spectroscopy. The single-source precursor provided control over the size and shape of the nanocrystals and ensured the stoichiometry of the product InSb quantum dots.

Using the new preparation method, we were able to make colloidal InSb quantum dots with diameters ranging from 3.2 ± 11% nm to 14.9 ± 6.4% nm. No other currently existing preparation method for colloidal InSb quantum dots offers access to such a wide range of sizes. EDX measurements showed that all quantum dots were stoichiometric regardless of their size. From electron diffraction and high-resolution TEM performed on the 14.9 nm-sized quantum dots we deduced that they have a wurtzite crystal structure.

We found that a number of variables played a crucial role in the InSb quantum dot synthesis. In order to obtain stoichiometric InSb quantum dots, it is of great importance that the reaction temperature exceeds 210 degrees. Additionally, the amount of reducing agent that is added during the synthesis could be varied to influence the size of the quantum dots. Finally, we found that prolongation of the time interval between addition of the reducing agent and the injection of the precursor solution significantly improves the quality of the product quantum dots.

From the absence of mass transport in our samples and the binomial size distribution of the product InSb quantum dots, we deduced that our system does not adhere to the classical nucleation and growth theory. Instead, we believe our samples grow through the collision and subsequent irreversible attachment of InSb units.

The size dependence of the quantum dot band gap energy was determined using steady-state absorption spectroscopy. By tuning the quantum dot sizes from 3.8 to 6.9 nm, we found that we could vary their band gap energy from roughly 1.11 to 0.81 eV. Transient absorption measurements indicated that photogenerated carriers in the InSb quantum dots are quickly localized in trap states. Nevertheless, we could observe a weak photoluminescence signal that was located at a spectral position that roughly matched the quantum dot band gap energy. Upon lowering the temperature to 4 K, the full width half maximum of the photoluminescence peak was greatly improved.

Although a number of conclusions can be formulated from this research, many questions still remain. Observations such as the colour change of oleylamine upon injection of the reducing agent and the great significance of the time interval between addition of the reducing agent and injection of the precursor solution are still not understood. Moreover, our results obtained on the influence of reaction time on the product quantum dots are still inconclusive. In order to further optimize the preparation method, we need to increase our understanding of the reaction mechanism.

Furthermore, our dataset regarding the synthetized quantum dots is still incomplete. So far, we have elucidated the crystal structure of only the 14.9 nm-sized quantum dots. The crystal structure of quantum dots that are smaller than 14.9 nm could be determined using high resolution TEM. Moreover, due to the difficulty of performing absorption spectroscopy in the infrared region of the electromagnetic spectrum, the band gap energies of quantum dots bigger than 7 nm could not be obtained using the spectrophotometer. An alternative way to probe their quantum dot band gap is through scanning tunnelling spectroscopy. An additional advantage of scanning tunnelling

spectroscopy is that single quantum dots are measured, and therefore the size distribution of the sample becomes irrelevant.

Due to the large electron mobility of bulk InSb, it may be interesting to investigate the mobility of the charge carriers in the colloidal InSb quantum dots. This mobility can be measured performing THz spectroscopy on solid InSb quantum dot films.

Transient absorption and photoluminescence measurements indicated that charge carriers are easily localized at trap states. Since these trap states often originate from surface states, the optical properties of the quantum dots may be improved by overgrowth of a heteroepitaxial shell. This shell can passivate the surface states and thereby promote the radiative combination of the exciton. Promising candidates for the shell material are CdTe and CdSe since their lattice mismatch with InSb is small. The lattice constant of InSb is 6.479 Å and the lattice constants of CdTe and CdSe are 6.482 Å and 6.050 Å, respectively.[36] Moreover, the InSb band gap (0.17 eV) lies entirely within the band gaps of both CdTe (1.44 eV) and CdSe (1.74 eV).[37]

This thesis describes how the ligands that are added to the reaction mixture can be used to tune the spherical shape of the nanocrystals towards peanut- and Mickey Mouse shapes, i.e. quantum dot dimers and trimers. These dimers and trimers may be investigated as being quantum dot molecules. Quantum molecules are an emerging field in nanoscience in which quantum-mechanical coupling and hybridization of energy levels between quantum dots are observed.

Finally, we observed that the quantum dots tend to form highly ordered hexagonal structures upon drying. This observation, together with the high electron mobility of InSb, makes colloidal InSb quantum dots very promising for oriented attachment experiments.

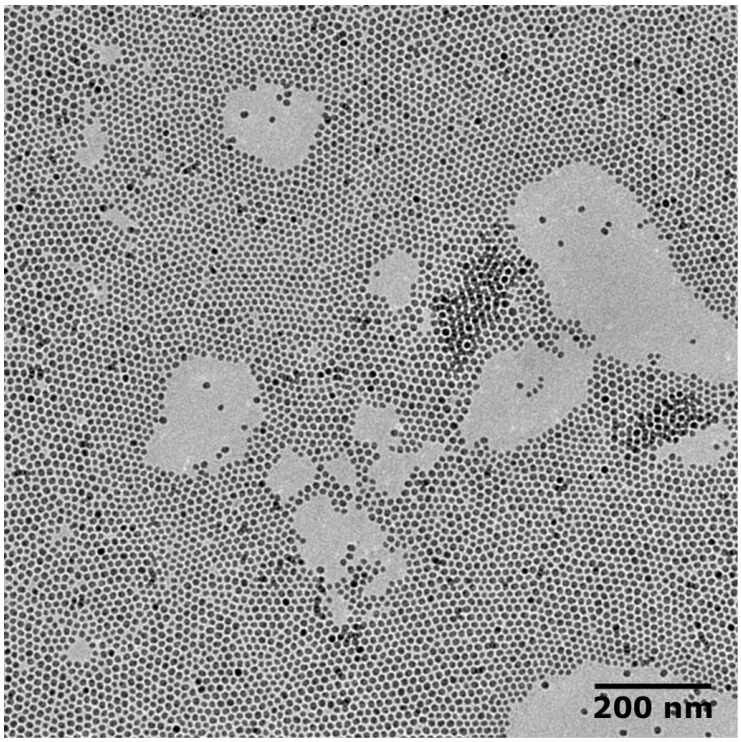

Figure 5.1: The colloidal InSb quantum dots are observed to form ordered hexagonal structures upon drying.

Samenvatting voor leken

Deze masterthesis beschrijft de colloïdale synthese van halfgeleider nanokristallen. Kristallen zijn materialen waarin de atomen periodiek gerangschikt zijn en samen een herhalend patroon vormen. Nanokristallen bevatten slechts een paar honderd tot een paar duizend atomen en hebben een grootte tussen de 1 en 100 nanometer, oftewel tussen de 0.000000001 en 0.0000001 meter. Dat is zo onvoorstelbaar klein dat ze niet zichtbaar zijn met het blote oog en er zelfs elektronenmicroscopen voor nodig zijn om de deeltjes te kunnen bekijken.

Een bijzondere eigenschap van halfgeleidermaterialen is dat ze licht met specifieke golflengten kunnen absorberen. Wanneer dit gebeurt gebruikt het materiaal de energie van het geabsorbeerde licht om een zogenaamd exciton te creëren. De grootte van het exciton hangt af van het type halfgeleidermateriaal waarvan het deeltje gemaakt is. Het kan zijn dat de diameter van een halfgeleider nanokristal kleiner is dan de grootte van het exciton. Aangezien het exciton niet buiten het nanokristal kan treden zal het zich dan moeten samendrukken. Dit fenomeen heet quantum confinement. Nanokristallen die quantum confinement ondervinden worden ook wel quantum dots genoemd.

Het is intuïtief dat quantum confinement een energie met zich meebrengt die groter wordt wanneer de deeltjes kleiner worden. Deze energie brengt grote veranderingen teweeg in de elektronische structuur van de deeltjes. Een resultaat daarvan is dat quantum dots met verschillende groottes licht met verschillende golflengten kunnen absorberen. Op basis van deze eigenschap kan de golflengte waarop de deeltjes licht absorberen afgesteld worden door middel van de deeltjesgrootte. Daardoor worden quantum dots uitermate geschikt geacht voor toepassing in verschillende soorten apparatuur, zoals bijvoorbeeld in zonnepanelen.

De quantum dots zijn doorgaans colloïden, wat betekent dat ze stabiel zijn in vloeistoffen. De synthese van colloïdale quantum dots is een uitdagende onderneming. Om de eigenschappen van de quantum dots het beste tot hun recht te laten komen moeten de groottes van de deeltjes zo veel mogelijk gelijk zijn. Ook moeten de deeltjes stoïchiometrisch zijn, wat inhoudt dat de twee verschillende atoomsoorten van het halfgeleidermateriaal in gelijke hoeveelheden in het deeltje aanwezig zijn. Ten slotte moeten de quantum dots een kristalstructuur hebben en gelijk van vorm zijn.

In deze thesis wordt een nieuwe manier gepresenteerd om quantum dots te maken van het halfgeleidermateriaal indium antimonide (InSb). Omdat indium en antimonide zo dicht bij elkaar staan in het periodiek systeem heeft InSb zeer bijzondere eigenschappen. Zo is InSb de halfgeleider die het allersnelst stroom kan geleiden. Ook is de grootte van het exciton dat InSb creëert onder absorptie van licht groter dan bij andere halfgeleiders. Dat betekent dat relatief grote InSb nanokristallen ook quantum confinement kunnen ondervinden. Daardoor kan de golflengte waarop InSb quantum dots licht absorberen gevariëerd worden over een erg breed bereik.

Omdat indium en antimonide zo dicht bij elkaar liggen in het periodiek systeem is het moeilijk om deze twee soorten elementen op een gecontroleerde manier met elkaar te laten binden. Om die reden is er tot op heden slechts weinig onderzoek gedaan naar colloïdale InSb quantum dots. De bestaande methoden om colloïdale InSb quantum dots te maken zijn gebaseerd op chemicaliën die niet te koop zijn en dus eerst zelf gesynthetiseerd moeten worden. De methode die in deze thesis beschreven wordt maakt uitsluitend gebruik van chemicaliën die kant en klaar bij leveranciers te koop zijn. Een ander voordeel van deze methode is dat het gebruik maakt van een precursoroplossing waarin indium- en antimonide-atomen in paren aan elkaar gebonden zijn. Deze

indium-antimonide complexen bieden niet alleen controle over het vormingsproces van de quantum dots, ook zijn de resulterende quantum dots altijd stoïchiometrisch.

Tijdens het uitvoeren van de syntheses observeerden we dat de vorming van colloïdale InSb quantum dots vaak afweek van de manier waarop we dit kennen voor quantum dots van andere halfgeleidermaterialen. Daarom werden de parameters van de synthese systematisch veranderd en de invloed daarvan bestudeerd. Vervolgens hebben we geprobeerd te beschrijven hoe het vormingsproces van InSb quantum dots dan wél in elkaar steekt.

De nieuwe synthesemethode werd gebruikt om quantum dots te maken met diameters die uiteenlopen van 3 tot 15 nanometer. We slaagden erin om de groottes van de quantum dots in dezelfde oplossing min of meer identiek te krijgen. We bewezen dat de quantum dots inderdaad altijd stoïchiometrisch zijn, onafhankelijk van hun grootte. Met de hulp van elektronenmicroscopen ontrafelden we de kristalstructuur van de 15 nm grote quantum dots. Door absorptiemetingen te verrichten zagen we dat de golflengte van het licht dat de quantum dots absorberen inderdaad afhangt van de grootte van de quantum dots. Ook observeerden we dat de quantum dots dit licht vervolgens weer uit kunnen zenden.

Het werk dat wordt beschreven in deze masterthesis is pionierend onderzoek. Tijdens het onderzoek hebben we een aantal duidelijke conclusies weten te trekken, maar toch zijn er nog ontzettend veel dingen die ons niét duidelijk zijn. Daarom hebben we genoeg ideeën om verder onderzoek naar deze colloïdale InSb quantum dots mee in te vullen. Zo zouden we graag meer weten over het groeiproces van de quantum dots en willen we de kristalstructuur van de kleinere quantum dots achterhalen. Ook is het interessant om de geleiding van stroom door de quantum dots te meten. Ten slotte willen we proberen om een schil van een ander halfgeleidermateriaal over de InSb quantum dots heen te groeien om zo de eigenschappen van de quantum dots te verbeteren.

Acknowledgements

I would not have been able to achieve the results presented in this thesis without the help of a number of people. In this section, I would like to take the opportunity to thank those people.

First and foremost, I would like to thank my daily supervisor Serena. Over the past year, we have been working together very closely and the results presented in this thesis are a shared effort. I'm very proud of what we have achieved together! Thank you for your guidance and the countless hours you spent behind the multitude of electron microscopes. I wish you the best of luck with the next steps in (y)our research.

Celso, I would like to thank you for giving me the opportunity to do my MSc thesis in your group. You were very involved in the project and after our weekly meetings I always returned to the lab with many new ideas. Thank you for your supervision and for sharing your extensive knowledge on semiconductor nanocrystals!

A number of people have contributed to the microscopy and spectroscopic analysis of our samples. I would like to thank Johann Jastrzebski for helping us with NMR measurements. Hans Meeldijk, thank you for operating the TALOS microscope. Wiebke Albrecht and Sara Bals from EMAT Antwerp, thank you for analyzing our particles at the TITAN microscope. Finally, I would like to thank Jaco Geuchies for transient absorption measurements and Annelies Bok for photoluminescence measurements.

Bibliography

[1] Brus, L.E. “Electron-Electron and Electron-Hole Interactions in Small Semiconductor Crystallites: The Size Dependence of the Lowest Excited Electronic State.” *The Journal of Chemical Physics*, vol. 80, no. 9, 1984, pp. 4403–4409

[2] Berends, A.C. “Explorations in Nanoscale Copper Indium Sulfide: Synthesis, Structural Analysis, and Optical Properties of $CuInS_2$ Nanocrystals.” PhD thesis, *Utrecht University*, 2018.

[3] “Wat Is Quantum Dot TV?” *Samsung Uk*, 19 Apr. 2018, www.samsung.com/nl/i/televisie/quantum-dot-tv/.

[4] Liu, W., *et al.* “Colloidal InSb Nanocrystals.” *Journal of the American Chemical Society*, vol. 134, no. 50, 2012, pp. 20258–20261.

[5] Cardozo, G.O., and J.P. Rino. “Molecular Dynamics Calculations of InSb Nanowires Thermal Conductivity.” *Journal of Materials Science*, vol. 46, no. 3, 2010, pp. 629–633.

[6] Yarema, M., and M.V. Kovalenko. “Colloidal Synthesis of InSb Nanocrystals with Controlled Polymorphism Using Indium and Antimony Amides.” *Chemistry of Materials*, vol. 25, no. 9, 2013, pp. 1788–1792.

[7] Tamang, S., *et al.* “Synthesis of Colloidal InSb Nanocrystals via in Situ Activation of InCl3.” *Dalton Transactions*, vol. 44, no. 38, 2015, pp. 16923–16928.

[8] Crisp, R.W., *et al.* “Selective Antimony Reduction Initiating the Nucleation and Growth of InSb Quantum Dots.” *Nanoscale*, vol. 10, no. 23, 2018, pp. 11110–11116.

[9] Groeneveld, E., and C. De Mello Donegá. “Chapter 6: The Challenge of Colloidal Nanoparticle Synthesis.” *Nanoparticles: Workhorses of Nanoscience*, Springer, 2016, pp. 145–189.

[10] Manar, A., *et al.* “Characteristic Exciton Properties of ZnS and ZnSe Films.” *Materials Science and Engineering: B*, vol. 43, no. 1-3, 1997, pp. 121–125

[11] Groeneveld, E. “Synthesis and optical spectroscopy of (hetero)-nanocrystals: An exciting interplay between chemistry and physics.” PhD thesis, *Utrecht University*, 2012.

[12] De Mello Donegá, C. “Synthesis and Properties of Colloidal Heteronanocrystals.” *Chem. Soc. Rev.*, vol. 40, no. 3, 2011, pp. 1512–1546.

[13] Pound, G.M., and V.K. La Mer. “Kinetics of Crystalline Nucleus Formation in Supercooled Liquid Tin.” *Journal of the American Chemical Society*, vol. 74, no. 9, 1952, pp. 2323–2332.

[14] La Mer, V.K., and R.H. Dinegar. “Theory, Production and Mechanism of Formation of Monodispersed Hydrosols.” *Journal of the American Chemical Society*, vol. 72, no. 11, 1950, pp. 4847–4854.

[15] Wang, F., *et al.* “Kinetics and Mechanisms of Aggregative Nanocrystal Growth.” *Chemistry of Materials*, vol. 26, no. 1, 2013, pp. 5–21.

[16] Polte, J., *et al.* "Formation Mechanism of Colloidal Silver Nanoparticles: Analogies and Differences to the Growth of Gold Nanoparticles." *ACS Nano*, vol. 6, no. 7, 2012, pp. 5791–5802.

[17] De Roo, J., *et al.* "Highly Dynamic Ligand Binding and Light Absorption Coefficient of Cesium Lead Bromide Perovskite Nanocrystals." *ACS Nano*, vol. 10, no. 2, 2016, pp. 2071–2081.

[18] Baldwin, R.A., *et al.* "Synthesis and Characterization of Potential Single-Source Precursors to Group 13−Antimonides." *Organometallics*, vol. 15, no. 23, 1996, pp. 5035–5038.

[19] Stuart, B. *Infrared Spectroscopy: Fundamentals and Applications*. J. Wiley, 2004.

[20] Zheng, H., *et al.* "Observation of Single Colloidal Platinum Nanocrystal Growth Trajectories." *Science*, vol. 324, no. 5932, 2009, pp. 1309–1312.

[21] Shields, S.P., *et al.* "Nucleation Control of Size and Dispersity in Aggregative Nanoparticle Growth. A Study of the Coarsening Kinetics of Thiolate-Capped Gold Nanocrystals." *Chemistry of Materials*, vol. 22, no. 10, 2010, pp. 3212–3225.

[22] Chen, M., *et al.* "Preparation and Study of Polyacryamide-Stabilized Silver Nanoparticles through a One-Pot Process." *The Journal of Physical Chemistry B*, vol. 110, no. 23, 2006, pp. 11224–11231.

[23] Taubert, A., *et al.* "Dendrimer-Controlled One-Pot Synthesis of Gold Nanoparticles with a Bimodal Size Distribution and Their Self-Assembly in the Solid State." *Journal of Materials Chemistry*, vol. 13, no. 5, 2003, pp. 1090–1093.

[24] Efros, A.L., and M. Rosen. "Quantum Size Level Structure of Narrow-Gap Semiconductor Nanocrystals: Effect of Band Coupling." *Physical Review B*, vol. 58, no. 11, 1998, pp. 7120–7135.

[25] Xia, C., *et al.* "Size-Dependent Band-Gap and Molar Absorption Coefficients of Colloidal $CuInS_2$ Quantum Dots." *ACS Nano*, vol. 12, no. 8, 2018, pp. 8350–8361.

[26] Moreels, I., *et al.* "Size-Dependent Optical Properties of Colloidal PbS Quantum Dots." *ACS Nano*, vol. 3, no. 10, 2009, pp. 3023–3030.

[27] Moreels, I., *et al.* "Composition and Size-Dependent Extinction Coefficient of Colloidal PbSe Quantum Dots." *Chemistry of Materials*, vol. 19, no. 25, 2007, pp. 6101–6106.

[28] llan, G., and C. Delerue. "Confinement Effects in PbSe Quantum Wells and Nanocrystals." Physical Review B, vol. 70, no. 24, 2004, p. 245321.

[29] Berera, R., *et al.* "Ultrafast Transient Absorption Spectroscopy: Principles and Application to Photosynthetic Systems." *Photosynthesis Research*, vol. 101, no. 2-3, 2009, pp. 105–118.

[30] Sher, P.H., *et al.* "Power Law Carrier Dynamics in Semiconductor Nanocrystals at Nanosecond Timescales." *Applied Physics Letters*, vol. 92, no. 10, 2008, p. 101111.

[31] Chang, A.Y., *et al.* "Carrier Dynamics in Highly Quantum-Confined, Colloidal Indium Antimonide Nanocrystals." *ACS Nano*, vol. 8, no. 8, 2014, pp. 8513–8519.

[32] Guo, Q., and A. Yoshida. "Temperature Dependence of Band Gap Change in InN and AlN." *Japanese Journal of Applied Physics*, vol. 33, no. Part 1, No. 5A, 1994, pp. 2453–2456.

[33] Hauschild, R., *et al.* "Temperature Dependent Band Gap and Homogeneous Line Broadening of the Exciton Emission in ZnO." *Physica Status Solidi (c)*, vol. 3, no. 4, 2006, pp. 976–979.

[34] Teissier, R., *et al.* "Temperature-Dependent Valence Band Offset and Band-Gap Energies of Pseudomorphic GaAsSb on GaAs." *Journal of Applied Physics*, vol. 89, no. 10, 2001, pp. 5473–5477.

[35] Littler, C.L., and D.G. Seiler. "Temperature Dependence of the Energy Gap of InSb Using Nonlinear Optical Techniques." *Applied Physics Letters*, vol. 46, no. 10, 1985, pp. 986–988.

[36] "Lattice Constants." EESemi, 2004, eesemi.com/lattice_constants.htm.

[37] Kittel, C. "Chapter 8: Semiconductor Crystals." *Introduction to Solid State Physics*, Wiley, 2018, pp. 185–220.

Appendix A

NMR spectroscopy on the precursor solution

^{1}H NMR spectra

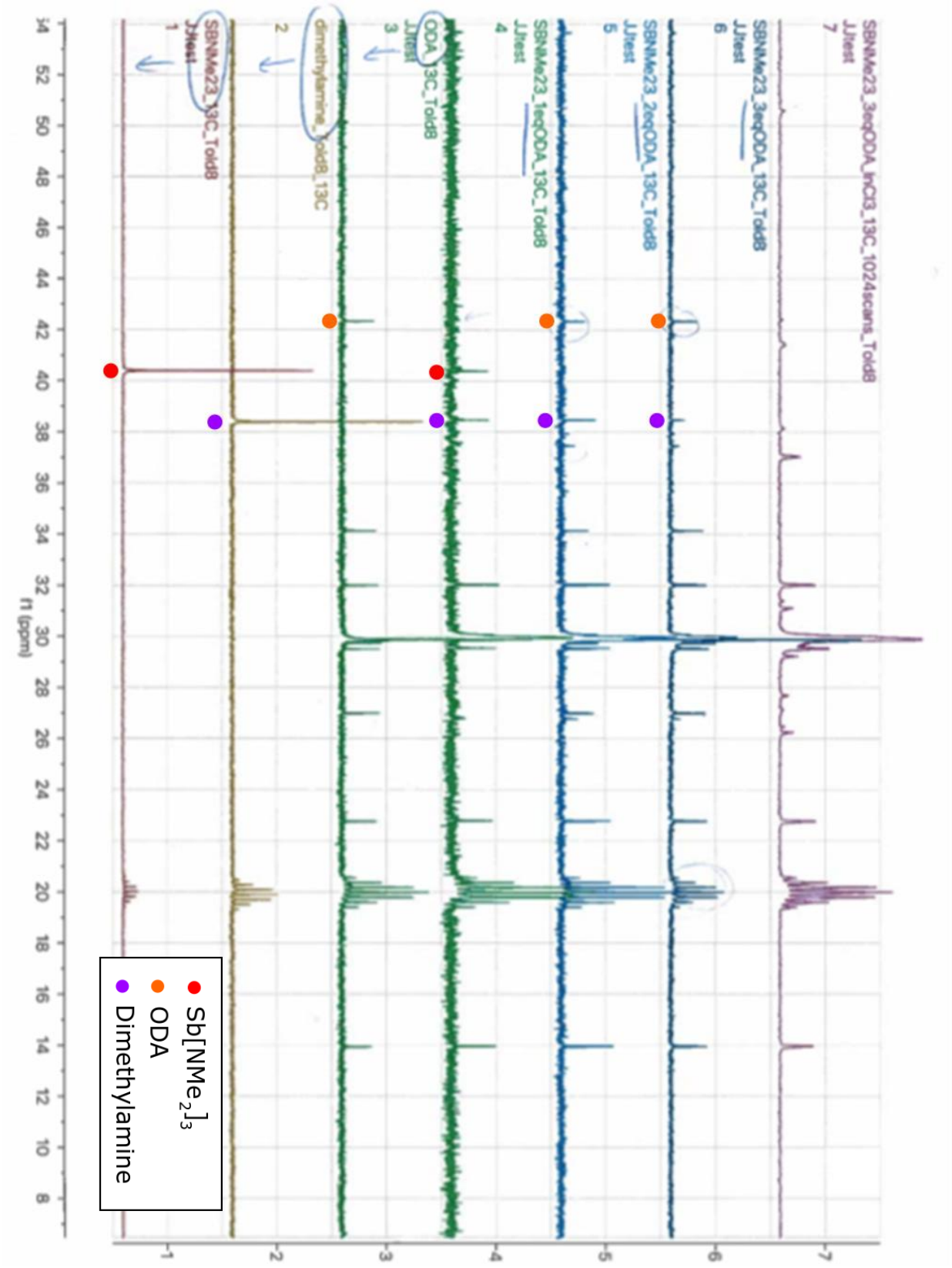

^{13}C NMR spectra

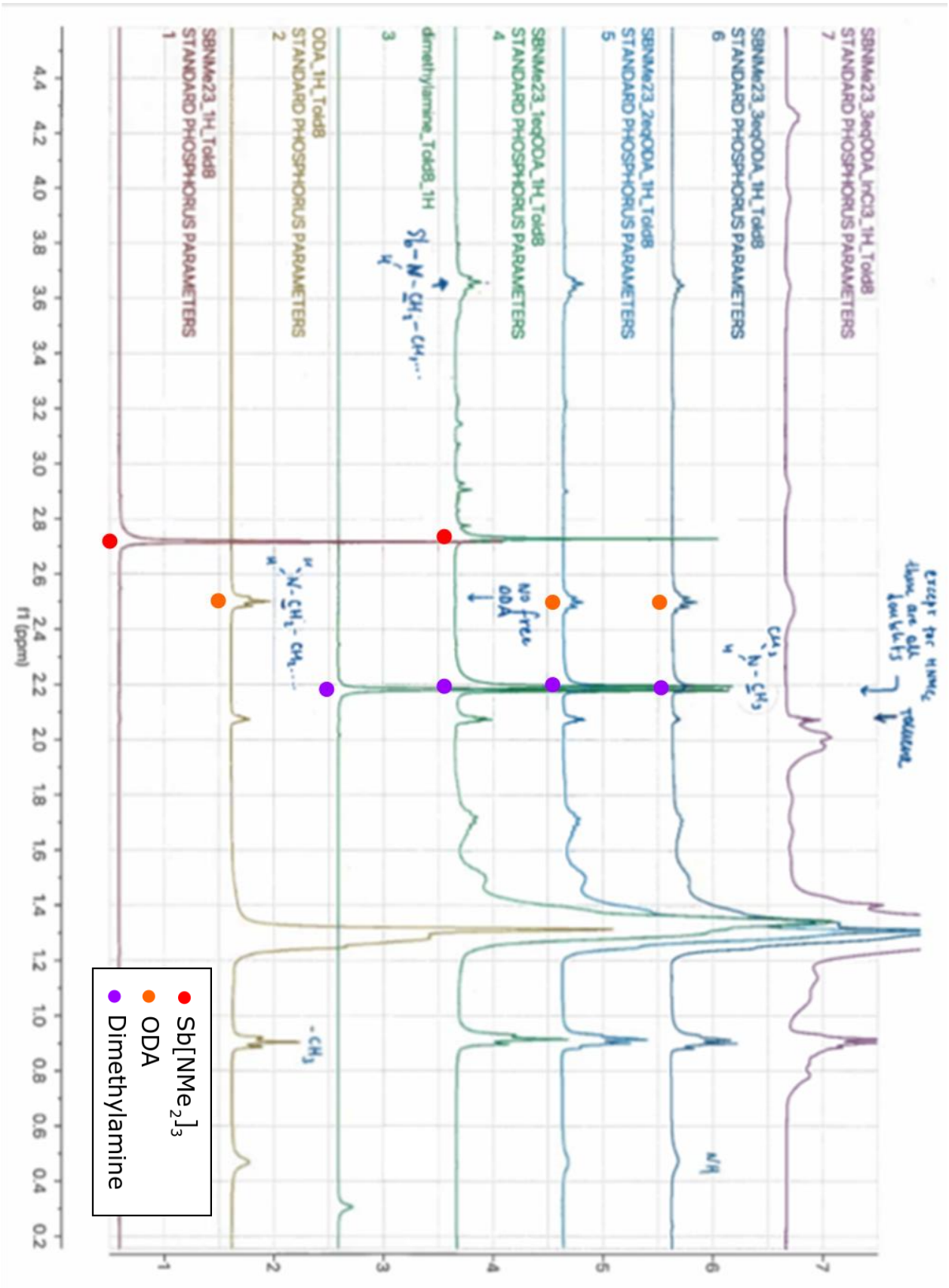

Appendix B

Reproducibility of the synthesis

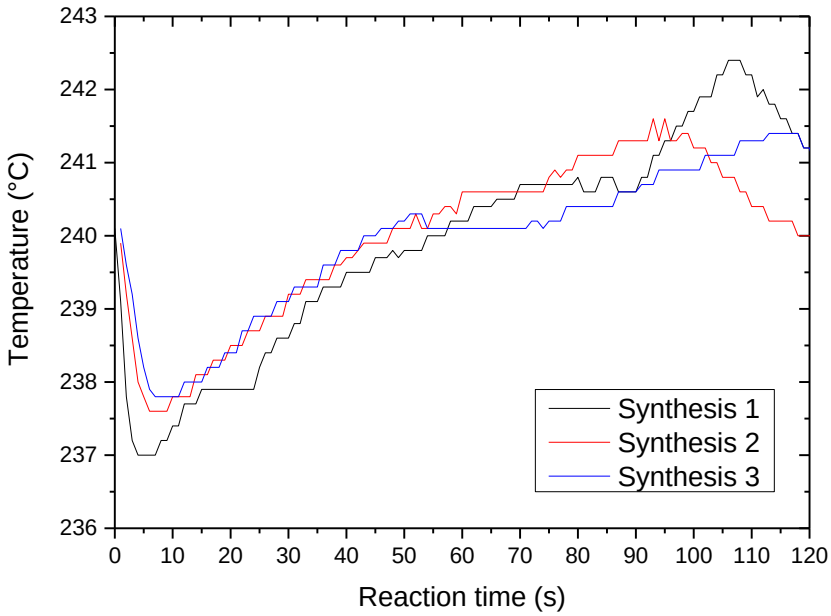

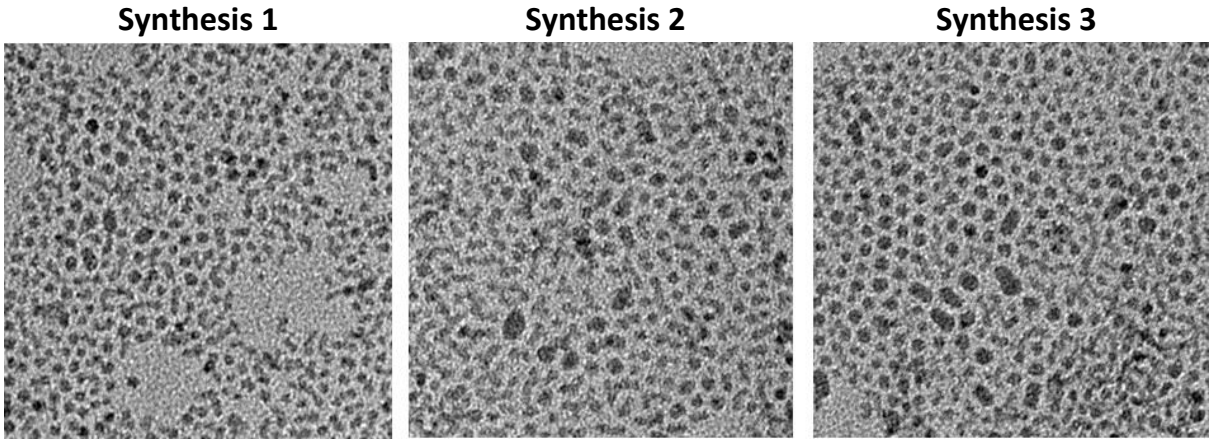

41% In 59% Sb | 51% In 49% Sb | 39% In 61% Sb

Three syntheses were carried out in which all reaction parameters were kept constant. The graph shows that the reaction temperatures for three different synthesis were nearly identical. The TEM images and elemental compositions of the reaction products were similar.

Appendix C

Independent nucleation and growth of In and Sb nanoparticles at low reaction temperatures

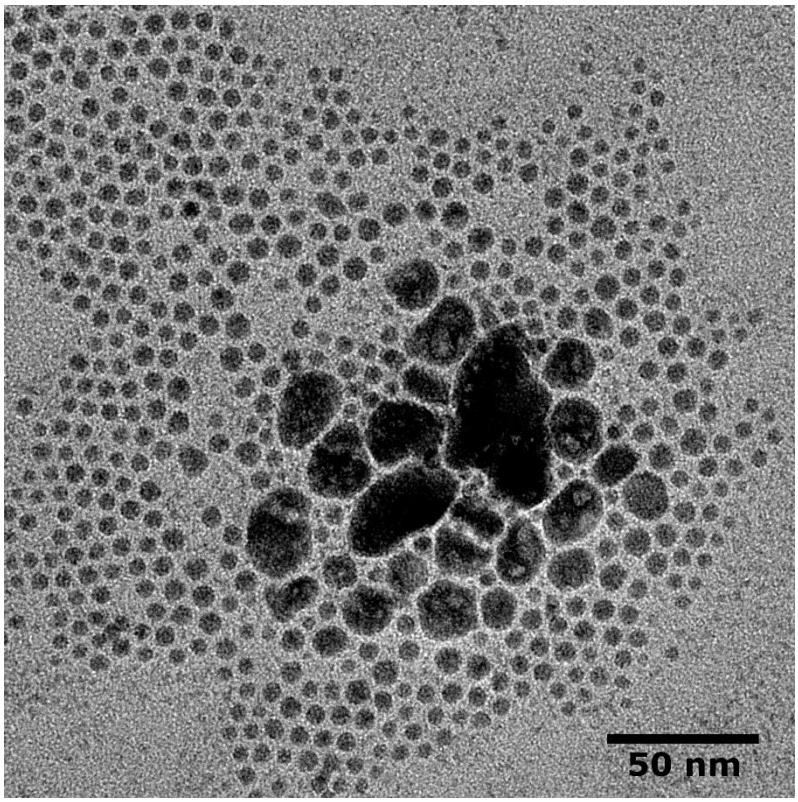

The TEM image shows a sample that was synthesized at a reaction temperature of 210 °C. It contained quantum dots composed of 80% In and 20% Sb with a diameter of 6.2 nm ± 10% and irregularly shaped particles composed of 15% In and 85% Sb with diameters ranging from 10 to 50 nm.

Appendix D

Tuning the quantum dot size by the amount of reducing agent

Quantum dots prepared using
mol(**In**):mol(**reducing agent**) = **1:9**

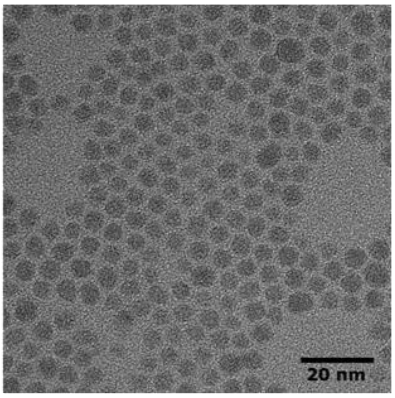

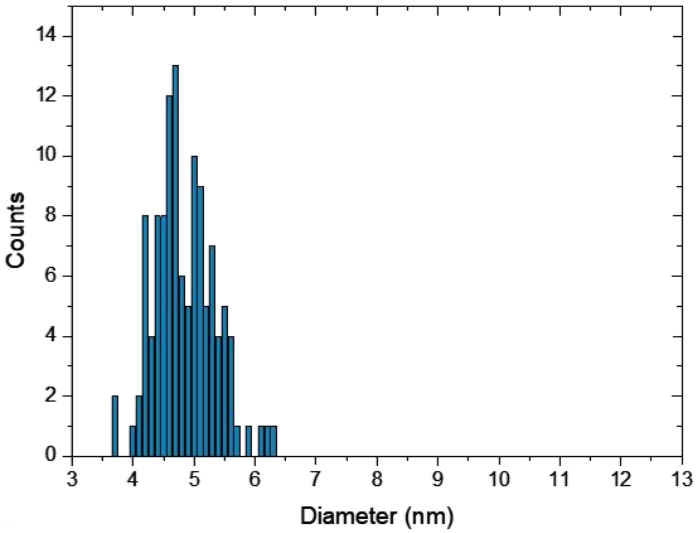

Quantum dots prepared using
mol(**In**):mol(**reducing agent**) = **1:12**

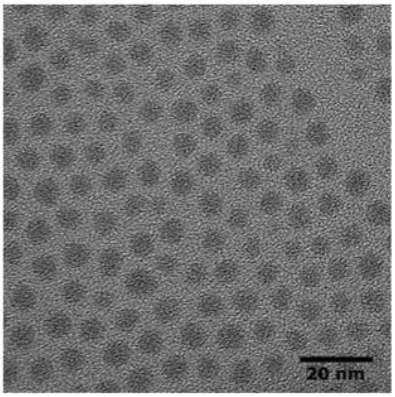

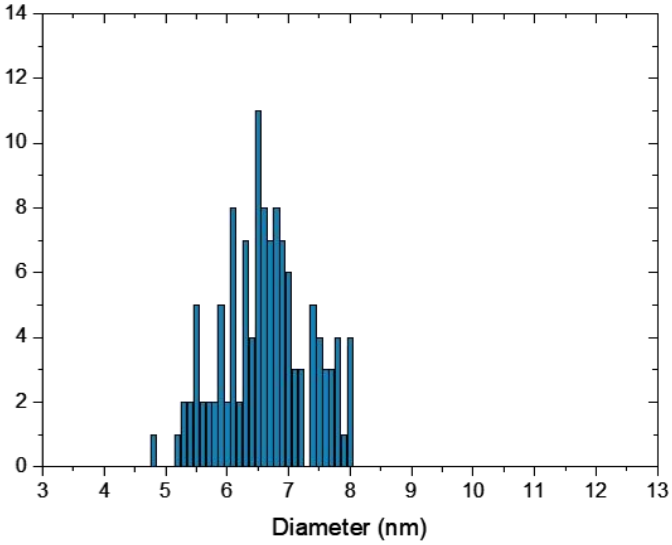

Quantum dots prepared using
mol(**In**):mol(**reducing agent**) = **1:15**

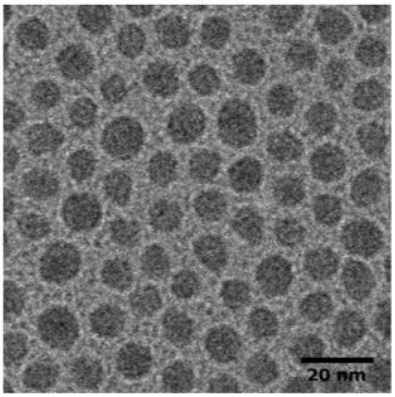

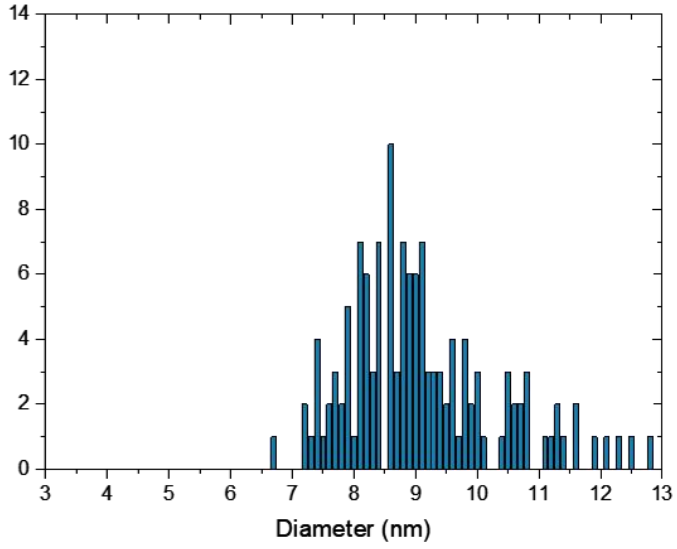

Appendix E

Influence of the time interval between addition of the reducing agent and the precursor injection on the reaction products

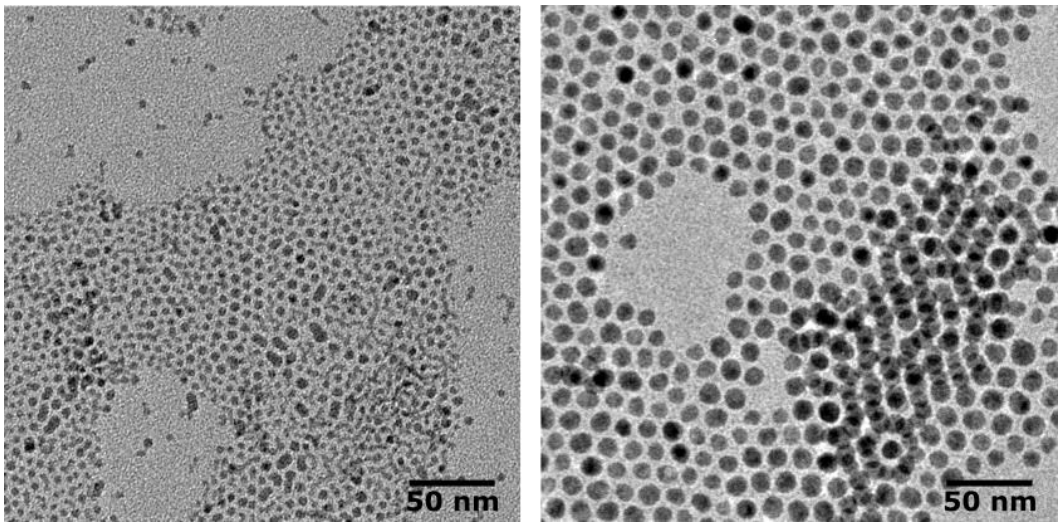

The left TEM image shows a sample that was prepared using a time interval between addition of the reducing agent and the injection of precursor solution of roughly 3 minutes. The right TEM image shows a sample that was prepared using a time interval of roughly 10 minutes.

Appendix F

Electron diffraction pattern of sub-15 nm InSb quantum dots

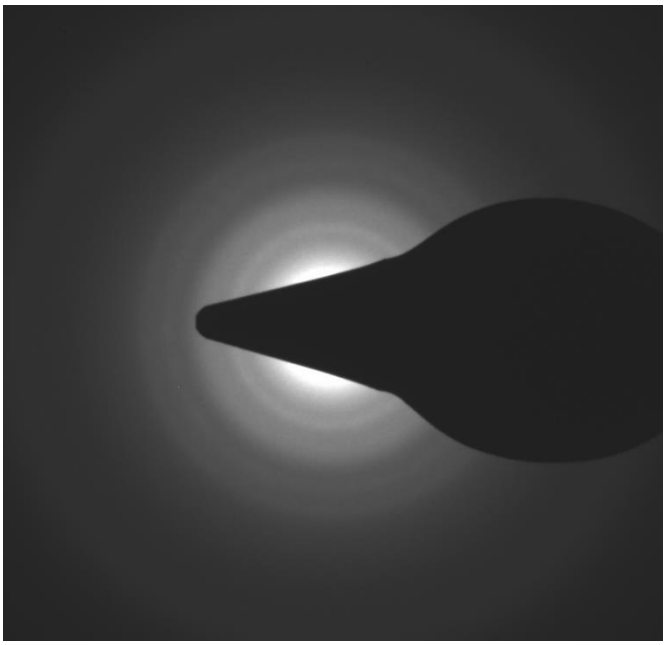

The bulk electron diffraction pattern of an ensemble of quantum dots with an average diameter of 9 nm. The pattern shows diffuse rings that do not allow for proper analysis.